Article

Targeting TRIM37-driven centrosome dysfunction in 17q23-amplified breast cancer

https://doi.org/10.1038/s41586-020-2690-1

Received: 10 June 2019

Accepted: 17 June 2020

Published online: 9 September 2020

Check for updates

Zhong Y. Yeow[1,2,6], Bramwell G. Lambrus[3,6], Rebecca Marlow[4,5], Kevin H. Zhan[3], Mary-Anne Durin[1,2], Lauren T. Evans[3], Phillip M. Scott[3], Thao Phan[3], Elizabeth Park[3], Lorena A. Ruiz[3], Daniela Moralli[2], Eleanor G. Knight[4], Luned M. Badder[5], Daniela Novo[4], Syed Haider[4], Catherine M. Green[2], Andrew N. J. Tutt[4,5], Christopher J. Lord[4], J. Ross Chapman[1,2]✉ & Andrew J. Holland[3]✉

Genomic instability is a hallmark of cancer, and has a central role in the initiation and development of breast cancer[1,2]. The success of poly-ADP ribose polymerase inhibitors in the treatment of breast cancers that are deficient in homologous recombination exemplifies the utility of synthetically lethal genetic interactions in the treatment of breast cancers that are driven by genomic instability[3]. Given that defects in homologous recombination are present in only a subset of breast cancers, there is a need to identify additional driver mechanisms for genomic instability and targeted strategies to exploit these defects in the treatment of cancer. Here we show that centrosome depletion induces synthetic lethality in cancer cells that contain the 17q23 amplicon, a recurrent copy number aberration that defines about 9% of all primary breast cancer tumours and is associated with high levels of genomic instability[4–6]. Specifically, inhibition of polo-like kinase 4 (PLK4) using small molecules leads to centrosome depletion, which triggers mitotic catastrophe in cells that exhibit amplicon-directed overexpression of *TRIM37*. To explain this effect, we identify TRIM37 as a negative regulator of centrosomal pericentriolar material. In 17q23-amplified cells that lack centrosomes, increased levels of TRIM37 block the formation of foci that comprise pericentriolar material—these foci are structures with a microtubule-nucleating capacity that are required for successful cell division in the absence of centrosomes. Finally, we find that the overexpression of TRIM37 causes genomic instability by delaying centrosome maturation and separation at mitotic entry, and thereby increases the frequency of mitotic errors. Collectively, these findings highlight *TRIM37*-dependent genomic instability as a putative driver event in 17q23-amplified breast cancer and provide a rationale for the use of centrosome-targeting therapeutic agents in treating these cancers.

Many cancer cells can proliferate without centrosomes[7,8]. However, while evaluating the response of cell lines to centrosome loss, we discovered that MCF-7 human breast adenocarcinoma cells were hypersensitive to centrosome loss induced by treatment with the PLK4 inhibitor centrinone[7]. Progressive centrosome loss induced upon treatment with centrinone in MCF-7 cells (Extended Data Fig. 1a) blocked the proliferation of these cells within three days (Fig. 1a), and greatly reduced clonogenic survival (Fig. 1c). In non-transformed cells, centrosome depletion using centrinone leads to activation of the mitotic surveillance pathway, which triggers p53-dependent growth arrest through USP28 and 53BP1[7,9–13]. However, we found that the sensitivity of MCF-7 cells to centrinone treatment was independent of this pathway (Fig. 1a, Extended Data Fig. 1b).

We considered whether the genetic background of MCF-7 cells underlies their hypersensitivity to centrosome depletion induced by PLK4 inhibition. MCF-7 cells contain the 17q23 breast cancer amplicon, a 3–4-Mb recurrent copy number aberration found in about 9% of all primary breast cancer tumours[4,14]. The 17q23 amplification also represents the defining feature of IntClust1 tumours, a subset of primarily oestrogen-receptor (ER)-positive, luminal B-type breast cancers that was detected following the genomic and transcriptomic profiling of more than 2,000 primary breast tumours by the METABRIC (Molecular Taxonomy of Breast Cancer International Consortium) project[4,5,15]. Of the approximately 40 protein-coding genes located within the 17q23 amplicon[16–18], we noted the presence of *TRIM37*, a gene that has previously been implicated in centrosome function[11,19].

[1]Medical Research Council (MRC) Molecular Haematology Unit, Weatherall Institute of Molecular Medicine, University of Oxford, Oxford, UK. [2]Wellcome Centre for Human Genetics, University of Oxford, Oxford, UK. [3]Department of Molecular Biology and Genetics, Johns Hopkins University School of Medicine, Baltimore, MD, USA. [4]The Breast Cancer Now Toby Robins Breast Cancer Research Centre, The Institute of Cancer Research, London, UK. [5]The Breast Cancer Now Unit, King's College London, London, UK. [6]These authors contributed equally: Zhong Y. Yeow, Bramwell G. Lambrus. ✉e-mail: ross.chapman@imm.ox.ac.uk; aholland@jhmi.edu

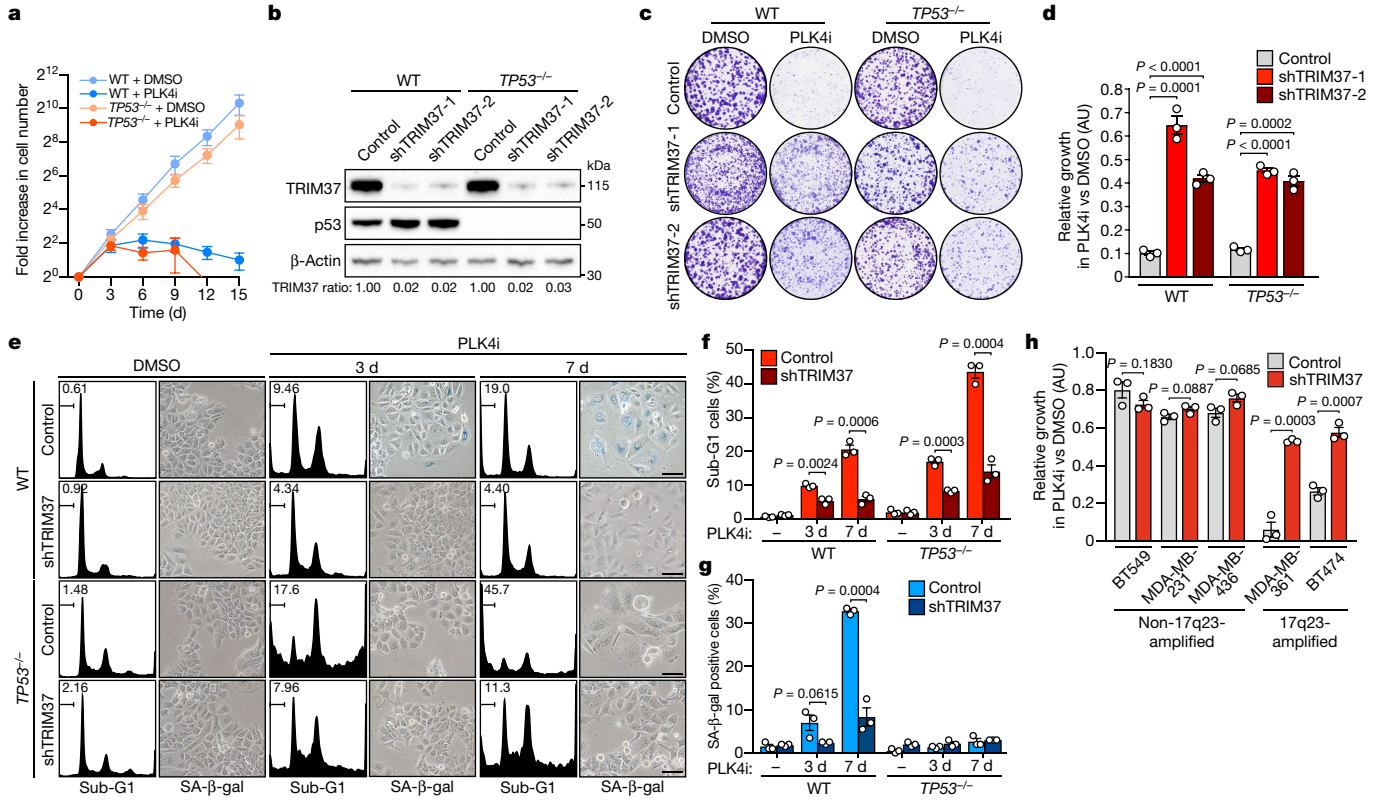

Fig. 1 | PLK4 inhibition is synthetically lethal with TRIM37 amplification. **a**, Fold increase in MCF-7 cell number after addition of centrinone (125 nM). $n = 3$ biological replicates. Mean ± s.e.m. WT, wild type. **b**, Immunoblot showing TRIM37 protein levels in wild-type and *TP53*$^{-/-}$ MCF-7 cells that stably express a control or one of two independent *TRIM37*-targeting shRNAs (shTRIM37-1 or shTRIM37-2). β-Actin, loading control. Representative data; $n = 3$ biological replicates. For gel source data, see Supplementary Fig. 1. **c**, Representative data of a 10-d clonogenic survival of indicated MCF-7 cell lines treated with DMSO (control) or centrinone (PLK4 inhibitor (PLK4i)) (125 nM). **d**, Quantification of **c**. $n = 3$ biological replicates. *P* values, unpaired two-tailed *t*-test. Mean ± s.e.m. **e**, MCF-7 cells treated with DMSO or centrinone (PLK4i) (125 nM) were analysed for DNA content, and stained for expression of senescence-associated β-galactosidase (SA-β-gal). Representative data of $n = 3$ biological replicates. Scale bars, 100 μm. **f**, Percentage of sub-G1 cells from **e**. $n = 3$ biological replicates. *P* values, unpaired two-tailed *t*-test. Mean ± s.e.m. –, DMSO treatment. **g**, Quantification of the percentage of SA-β-gal-positive cells from **e**. $n = 3$ biological replicates, each comprising ≥ 200 cells. *P* values, unpaired two-tailed *t*-test. Mean ± s.e.m. **h**, Quantification of clonogenic survival data for 17q23-amplified and non-17q23-amplified breast cancer cells transduced with a *TRIM37*-targeting shRNA or vector control and treated with DMSO or centrinone (PLK4i) (125 nM). $n = 3$ biological replicates. *P* values, unpaired two-tailed *t*-test. Mean ± s.e.m.

Knockout of TRIM37 leads to the accumulation of pericentriolar material (PCM) and accelerated spindle assembly in acentrosomal cells[11]. We therefore hypothesized that, conversely, high levels of TRIM37 could reduce PCM-mediated nucleation of microtubules, and thereby sensitize cells to centrosome loss. To test this, we transduced wild-type and *TP53*$^{-/-}$ MCF-7 cell lines with lentiviruses that encode control or *TRIM37*-targeting short hairpin RNAs (shRNAs), and monitored growth in the presence or absence of centrinone. In both cell lines, efficient TRIM37 depletion using two different shRNAs restored cell growth in the presence of centrinone, when compared to controls (Fig. 1b–d). Similarly, disruption of *TRIM37* with CRISPR–Cas9 conferred resistance to centrinone in two MCF-7 clones (Extended Data Fig. 1c–e). Treatment with centrinone induced senescence in MCF-7 cells, as evidenced by a time-dependent increase in cell flattening and senescence-associated β-galactosidase expression, or cell death, as marked by an accumulation of cells with a sub-G1 DNA content (Fig. 1e–g). Treatment with centrinone also inhibited the proliferation of *TP53*$^{-/-}$ MCF-7 cells, primarily by inducing cell death (Fig. 1e, f). Centrinone-induced senescence or cell death in MCF-7 cell lines was suppressed by the depletion of TRIM37 (Fig. 1e–g), which suggests that increased expression of *TRIM37* expression is synthetically lethal with PLK4 inhibition.

To test whether TRIM37 overexpression sensitizes cells to PLK4 inhibition, control (*eGFP*) or *TRIM37* transgenes were introduced into HCT116, a human colorectal carcinoma cell line that is insensitive to centrosome loss[7]. Overexpression of TRIM37 at levels comparable to those in MCF-7 cells (Extended Data Fig. 1f) inhibited clonogenic survival in centrinone-treated HCT116 cells, but only modestly affecting the growth of controls treated with dimethyl sulfoxide (DMSO) (Extended Data Fig. 1g, h). To ascertain whether the synthetically lethal effect of centrinone was specific to PLK4 inhibition, we overexpressed *TRIM37* in *PLK4*^{AS} *TP53*$^{-/-}$ RPE-1 cells, which exclusively express analogue-sensitive (AS) PLK4[13]. In these cells, neither doxycycline-induced *TRIM37* overexpression alone nor the inhibition of analogue-sensitive PLK4 with the bulky ATP analogue 3MB-PP1 affected cell proliferation (Extended Data Fig. 1i–l). By contrast, treatment with 3MB-PP1 resulted in cell flattening and markedly reduced colony survival in *TRIM37*-overexpressing *PLK4*^{AS} *TP53*$^{-/-}$ RPE-1 cells, but not in cells that overexpress a control *GST* transgene (Extended Data Fig. 1i–l). This confirms that the specific inhibition of PLK4 can kill cells with increased *TRIM37* expression.

CFI-400945 is a PLK4 inhibitor that also targets aurora B, and is in clinical trials as a therapeutic agent for patients with breast cancer[20–22]. We therefore tested the effect of CFI-400945 on the proliferation of MCF-7 cells. Treatment with centrinone, CFI-400945 or the aurora B inhibitor ZM44749 all potently inhibited clonogenic survival in MCF-7 cells (Extended Data Fig. 2a, b). However, depletion of TRIM37 restored only the proliferation of cells treated with centrinone—and not those treated with CFI-400945 or ZM447439. In cells treated with

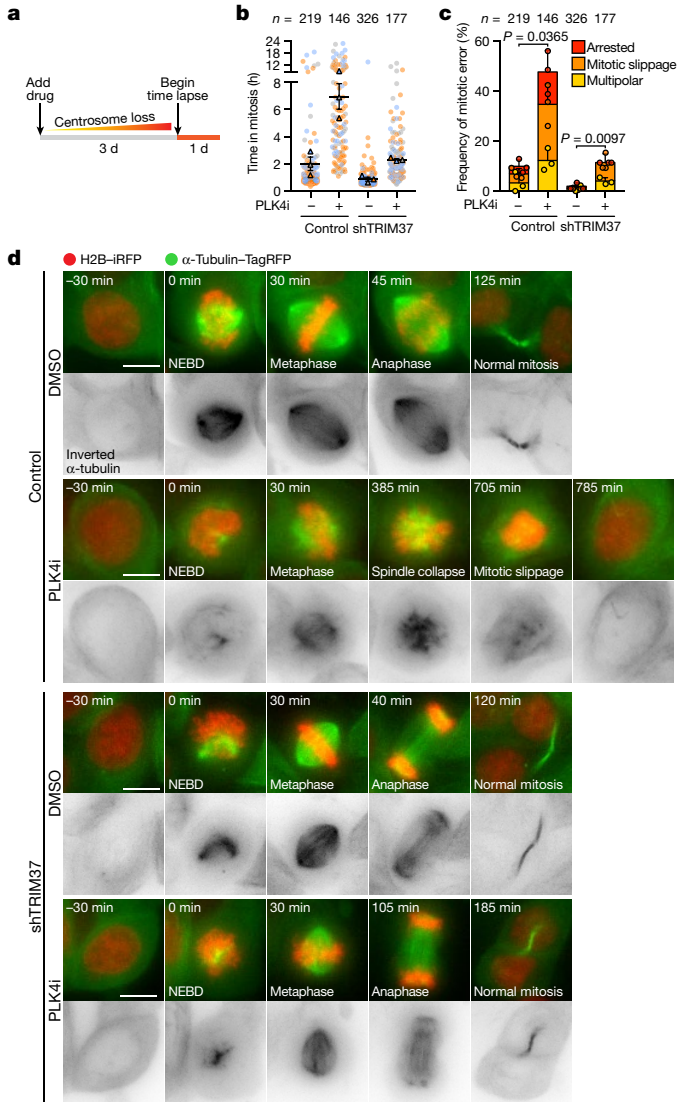

Fig. 2 | PLK4 inhibition triggers mitotic catastrophe in TRIM37-amplified cancer cells. a, Experimental schematic of time-lapse imaging of asynchronous cells. **b**, Quantification of mitotic duration in *TP53*$^{-/-}$ MCF-7 cells transduced with a control vector, compared to those expressing an shRNA targeting *TRIM37*. Cells were treated with DMSO (−) or centrinone (PLK4i) (125 nM) for 3 d before imaging. Triangles represent the mean for each biological replicate; coloured circles show individual data points from each of the replicates. Data acquired from $n = 3$ biological replicates, each with >40 cells. Mean ± s.e.m. **c**, Quantification of mitotic phenotypes from **b** in *TP53*$^{-/-}$ MCF-7 cells expressing control vector, compared to those expressing an shRNA targeting *TRIM37*. Data acquired from $n = 3$ biological replicates, each with >40 cells. *P* values, unpaired two-tailed *t*-test. Mean ± s.e.m. **d**, Representative time-lapse images of mitotic progression in DMSO- or centrinone (125 nM)-treated *TP53*$^{-/-}$ MCF-7 cells expressing control vector or *TRIM37*-targeting shRNA. Representative data; $n = 3$ biological replicates. Cells are labelled with H2B–iRFP and TagRFP–α-tubulin. NEBD, nuclear envelope break down. Scale bars, 5 µm.

CFI-400945 or ZM447439, analysis of DNA content revealed an accumulation of polyploid cells, which is a readout indicative of inhibition of aurora B kinase (Extended Data Fig. 2c). By contrast, treatment with centrinone did not increase the fraction of polyploid cells, consistent with the known selectivity of this compound for inhibiting PLK4 and not aurora B[7]. This shows that inhibitor selectivity towards PLK4—and not other kinases—is crucial for the synthetic lethal effect in cells that overexpress *TRIM37*.

To determine whether the cell killing induced by PLK4 inhibitors was common to 17q23-amplified breast cancer cell lines, we tested the effect of centrinone on the viability of BT474 and MDA-MB-361 (two additional 17q23-amplified breast cancer cell lines that overexpress *TRIM37*[16,23]), and compared their responses with those of a control panel of non-17q23-amplified breast cancer cell lines (BT549, MDA-MB-231 and MDA-MB-436) with normal TRIM37 expression (Extended Data Fig. 3a). As expected, PLK4 inhibition only minimally affected clonogenic survival across the control cell line panel, and TRIM37 depletion conferred no added resistance (Fig. 1h, Extended Data Fig. 3b). By contrast, both of the additional 17q23-amplified cell lines were hypersensitive to the PLK4 inhibitor; treatment with centrinone induced growth arrest, morphological aberrations and cell death (Fig. 1h, Extended Data Fig. 3b–d). These effects were also suppressed by stable knockdown of TRIM37, which confirms that the synthetically lethal effect of PLK4 inhibitor treatment depended on *TRIM37* overexpression in multiple 17q23-amplified cell lines.

To test whether TRIM37 overexpression was predictive for sensitivity to PLK4 inhibitors in patient-derived organoid models of breast cancer, we examined the centrinone sensitivity of 3D organoid cultures derived from patients with breast cancer with a high or low level of expression of *TRIM37* mRNA (Extended Data Fig. 3e). Expression of *TRIM37* mRNA was only partly predictive of TRIM37 protein levels (Extended Data Fig. 3g). Nevertheless, of four established cultures, two patient-derived organoids with high levels of TRIM37 protein—and one with an intermediate level of TRIM37 protein—were sensitive to nanomolar doses of centrinone. By contrast, a patient-derived organoid with low levels of TRIM37 protein remained insensitive to treatment with centrinone at concentrations below 1 µM (Extended Data Fig. 3f, g). The centrinone-sensitivity profiles of these patient-derived organoids resembled the 3D-culture responses of 17q23-amplified (MCF-7 and BT-474) and non-amplified (MDA-MB-231 and BT-549) breast tumour cell lines to centrinone treatment (Extended Data Fig. 3h). Taken together, our cell line and patient-derived-organoid experiments underscore the utility of PLK4-specific inhibitors in the killing of TRIM37-amplified breast cancer cells.

To investigate how PLK4 inhibition triggers growth defects in MCF-7 cells, we performed time-lapse microscopy to track the fates of control (DMSO)- and centrinone-treated *TP53*$^{-/-}$ MCF-7 cells (Fig. 2a, Supplementary Videos 1–4). Whereas control-treated cells progressed through mitosis normally, 47% of centrinone-treated cells formed short bipolar spindles that collapsed and remained arrested in mitosis or slipped out of mitosis without undergoing anaphase (Fig. 2b–d). Importantly, TRIM37 depletion rescued robust bipolar spindle formation in centrinone-treated MCF-7 cells, and almost completely reversed the effects of centrinone in prolonging mitosis and inducing cell division errors in MCF-7 cells (Fig. 2b–d). Thus, increased expression of *TRIM37* antagonizes spindle assembly in the absence of centrosomes, resulting in mitotic catastrophe.

To understand how TRIM37 inhibits spindle assembly, we identified proximity interaction partners by expressing mTurbo-tagged TRIM37 and performing proximity-dependent biotin labelling in RPE-1 cells[24,25]. After background subtraction, we identified 184 TRIM37 proximity-interaction partners, including 7 known interactors[26] (Extended Data Fig. 4a, c, Supplementary Data 1). Gene ontology analysis showed notable enrichment of centrosome proteins within these interactors (Extended Data Fig. 4b). This was corroborated by the localization of a pool of endogenous TRIM37 in close proximity to the centrosome, and the enrichment of biotinylated proteins at the centrosomes of RPE-1 cells expressing mTurbo–TRIM37 (Extended Data Fig. 4d, e). Among the most enriched proximity interactors of TRIM37 was CEP192, a core PCM component that accumulates in non-centrosomal foci in TRIM37-knockout cells[11]. The interaction between TRIM37 and CEP192 was confirmed by co-immunoprecipitation (Extended Data Fig. 4f). Neither histone H2A nor the peroxisome protein PEX5—two previously

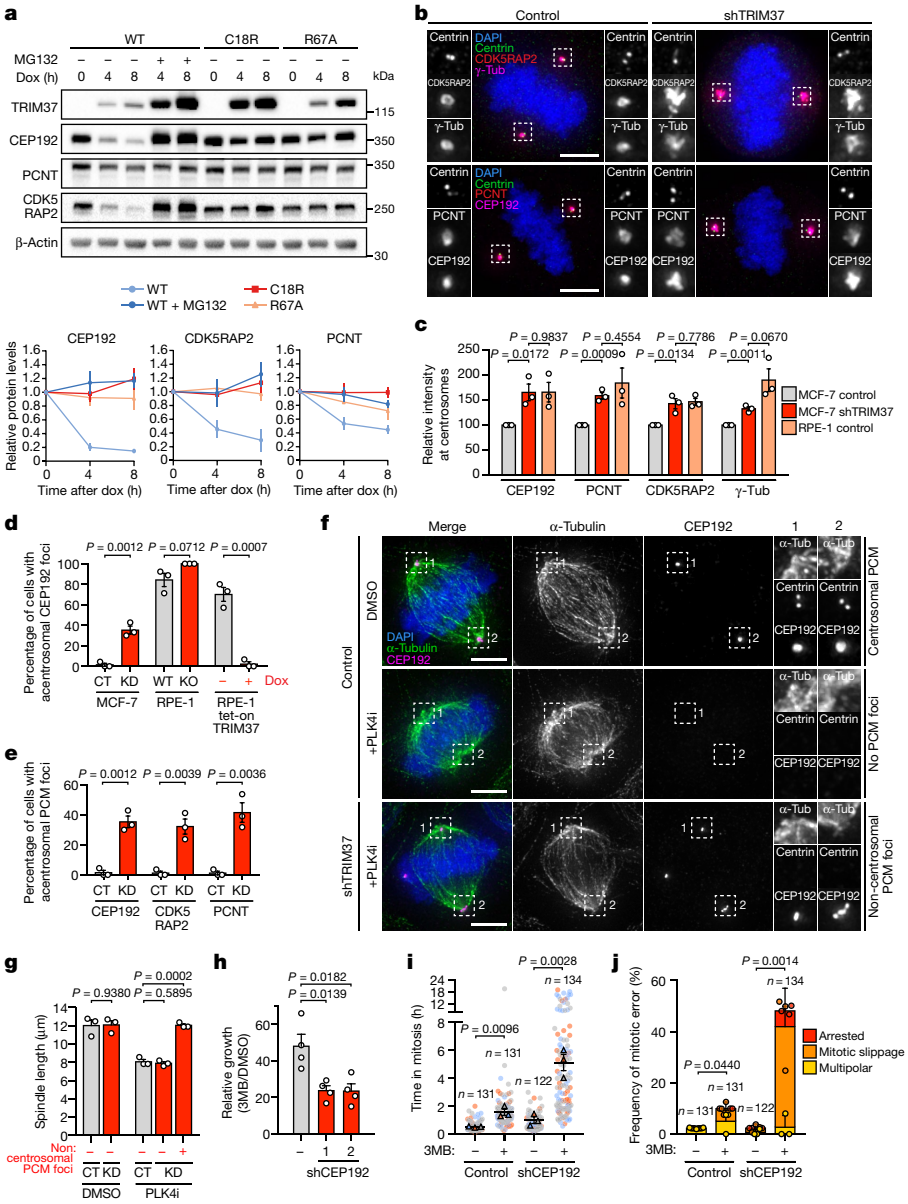

Fig. 3 | PCM sequestration by TRIM37 drives mitotic catastrophe in acentrosomal cells. a, Top, immunoblot showing PCM levels after overexpression of wild-type TRIM37 (WT), the RING-domain mutant TRIM37(C18R) or the ubiquitin-transfer-defective mutant TRIM37(R67A) in RPE-1 tet-on TRIM37 cells. β-Actin, loading control. For gel source data, see Supplementary Fig. 1. Bottom, normalized PCM levels relative to 0 h, representative of $n = 3$ biological replicates. Mean ± s.e.m. Dox, doxycycline. **b**, Centrosomal PCM levels in mitotic MCF-7 cells transduced with control vector or *TRIM37*-targeting shRNA. Representative images, $n = 3$ biological replicates. Scale bars, 5 μm. γ-Tub, γ-tubulin. **c**, Quantification of centrosomal PCM signal in mitotic cells. $n = 3$ biological replicates. *P* values, unpaired two-tailed *t*-test. Mean ± s.e.m. **d**, Quantification of mitotic CEP192 foci in centrinone-treated cells that lack centrosomes. $n = 3$, biological replicates, each comprising >30 cells. *P* values, unpaired two-tailed *t*-test. Mean ± s.e.m. CT, control vector; KD, knockdown with *TRIM37* shRNA; KO, *TRIM37* knockout. **e**, Quantification of mitotic PCM foci in centrinone-treated cells that lack centrosomes. $n = 3$ biological replicates, each comprising >30 cells. *P* values, unpaired two-tailed *t*-test. Mean ± s.e.m. **f**, Representative images for **e**. Scale bars, 5 μm. **g**, Quantification of mitotic spindle length in MCF-7 cells expressing control vector or *TRIM37*-targeting shRNA. $n = 3$ biological replicates, each comprising >10 cells. *P* values, unpaired two-tailed *t*-test. Mean ± s.e.m. **h**, Growth of 3MB-PP1 (3MB)-treated *PLK4*^{AS} *TP53*$^{-/-}$ RPE-1 cells expressing control vector or one of two *CEP192*-targeting shRNAs, relative to treatment with DMSO. $n = 4$ biological replicates. *P* values, unpaired two-tailed *t*-test. Mean ± s.e.m. **i**, Mitotic duration of the cells described in **h**, expressing H2B–eGFP and TagRFP–tubulin. Cells were grown in DMSO or 3MB-PP1 for 3 d before imaging. Triangles, mean for each biological replicate; coloured circles, individual data points from each replicate. $n = 3$ biological replicates, each comprising >30 cells. *P* values, unpaired two-tailed *t*-test. Mean ± s.e.m. **j**, Frequency of mitotic errors quantified in the samples as described in **i**. $n = 3$ biological replicates, each comprising >30 cells. *P* values, unpaired two-tailed *t*-test. Mean ± s.e.m.

reported substrates of TRIM37[23,27]—were among the labelled interactors, which confirms that centrosome proteins are primary TRIM37 proximity-interaction partners.

To test whether TRIM37 regulates the abundance of PCM proteins, we monitored the effect of altered TRIM37 expression on the cell-wide levels of three PCM scaffolding proteins: CEP192, PCNT and CDK5RAP2. Acute overexpression of *TRIM37* in RPE-1 cells markedly reduced the abundance of all three PCM proteins (Fig. 3a). Proteasome blockade with MG132 prevented the reduction in PCM protein abundance, which suggests that TRIM37 directs the degradation of these proteins via the ubiquitin-proteasome pathway. Consistent with this, the E3 ligase activity of TRIM37 was critical for PCM protein degradation, as both

catalytically inactive (C18R)[23,27] and predicted ubiquitin-binding- and transfer-defective (R67A)[28] RING domain mutants of TRIM37 did not reduce levels of the PCM proteins (Fig. 3a). Having established that TRIM37 directs PCM protein proteolysis, we next investigated whether 17q23-amplification status correlated with reduced PCM levels. We found that the 17q23-amplified cell lines with TRIM37 overexpression have lower cell-wide levels of CEP192, PCNT and CDK5RAP2 compared to their non-17q23-amplified counterparts (Extended Data Fig. 4g). The levels of CEP192, PCNT and CDK5RAP2 were also reduced at mitotic centrosomes in MCF-7 cells, but restored following TRIM37 depletion to levels comparable to those seen in RPE-1 cells (Fig. 3b, c). Microtubule regrowth assays showed that mitotic centrosomes in TRIM37-depleted MCF-7 cells nucleated nearly twice the amount of α-tubulin compared to the control cells (Extended Data Fig. 5a, b). Similarly, the levels of EB1, a plus-end tracking marker of growing microtubules, were increased by more than threefold at the centrosomes of TRIM37-depleted cells (Extended Data Fig. 5a, c).

Fixed-cell analysis revealed that acentrosomal RPE-1, DLD-1 and MDA-MB-436 cells that express low levels of TRIM37 formed PCM aggregates in more than 80% of mitotic cells. However, these PCM foci were absent from MCF-7 cells and from TRIM37-overexpressing RPE-1 cells (Fig. 3d–f, Extended Data Fig. 5d, e). We therefore asked whether the role of TRIM37 in controlling PCM abundance could modulate the assembly of non-centrosomal PCM foci. Depleting TRIM37 enabled the formation of PCM foci in acentrosomal MCF-7 cells (Fig. 3d–f) and increased the penetrance and size of these structures in acentrosomal RPE-1 cells (Fig. 3d, Extended Data Fig. 5d, f). Centrosome loss also reduced the length of the mitotic spindle in MCF-7 cells (Fig. 3g, Extended Data Fig. 5g). However, TRIM37 depletion enabled acentrosomal MCF-7 cells with PCM foci to generate spindle lengths that matched those of untreated MCF-7 cells. Thus, *TRIM37* overexpression suppresses the formation of non-centrosomal PCM foci, which leads to defects in spindle assembly.

To define the spatial and temporal assembly properties of non-centrosomal PCM foci, we generated DLD-1 cells that express endogenously tagged CEP192–mNeonGreen to mark PCM. In DMSO-treated control DLD-1 cells, CEP192–mNeonGreen localized to the centrosomes in interphase and increased in intensity by about threefold during mitosis (Extended Data Fig. 6a, Supplementary Video 5). By contrast, CEP192–mNeonGreen was diffusely localized in acentrosomal DLD-1 cells throughout interphase but assembled into multiple non-centrosomal PCM foci during early prometaphase (Extended Data Fig. 6b, Supplementary Video 6). These PCM foci coalesced into spindle poles at metaphase, and subsequently disassemble upon mitotic exit.

Non-centrosomal PCM foci often resided at the centre of microtubule asters (Extended Data Fig. 5d, e, g). To examine whether these structures could promote microtubule nucleation, we performed live-cell confocal imaging on acentrosomal DLD-1 cells that express endogenously tagged CEP192–mNeonGreen and EB1–TagRFP. In DMSO-treated control cells, EB1–TagRFP tracked the growing ends of microtubules nucleated by the centrosomes (Extended Data Fig. 6c, Supplementary Video 7). In acentrosomal DLD-1 cells, non-centrosomal PCM foci nucleated microtubules and were incorporated into the mitotic spindle (Extended Data Fig. 6d, Supplementary Video 8). Importantly, microtubule nucleation by non-centrosomal PCM foci preceded their incorporation into the spindle (Extended Data Fig. 6e, Supplementary Video 9). Similar results were obtained with acentrosomal RPE-1 cells that co-express EB3–mNeonGreen to track the plus-end tip of microtubules and γ-tubulin–TagRFP to mark acentrosomal PCM foci (Extended Data Fig. 7, Supplementary Videos 10–14). We conclude that, in cells that lack centrosomes, non-centrosomal PCM foci form specifically in mitosis and are required for efficient microtubule nucleation and robust bipolar spindle assembly.

To test whether PCM depletion could explain the synthetically lethal effect of centrosome loss in cells with *TRIM37* overexpression, we depleted the TRIM37 target CEP192 in *PLK4*^{AS} *TP53*$^{-/-}$ RPE-1

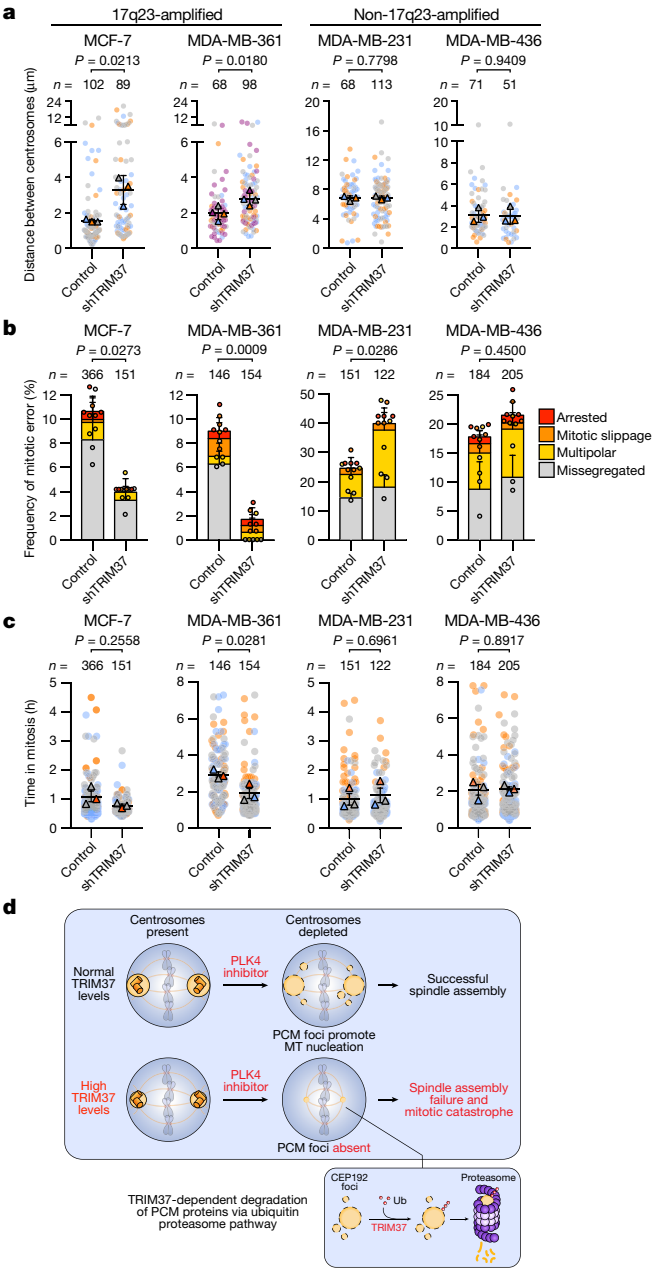

Fig. 4 | TRIM37 overexpression delays centrosome separation in late G2 phase, and promotes mitotic errors. a, Quantification of the distance between the two centrosomes at NEBD in MCF-7, MDA-MB-361, MDA-MB-231 and MDA-MB-436 cells expressing a control vector, compared to those expressing an shRNA targeting *TRIM37*. Data acquired from $n \geq 3$ biological replicates, each with 8–45 cells. *P* values, unpaired two-tailed *t*-test. Mean ± s.e.m. **b**, Quantification of mitotic phenotypes in MCF-7, MDA-MB-361, MDA-MB-231 and MDA-MB-436 cells expressing a control vector, compared to those expressing an shRNA targeting *TRIM37*. Data acquired from $n = 3$ biological replicates, each with >40 cells. *P* values, unpaired two-tailed *t*-test. Mean ± s.e.m. **c**, Quantification of mitotic duration in MCF-7, MDA-MB-361, MDA-MB-231 and MDA-MB-436 cells expressing a control vector, compared to those expressing an shRNA targeting *TRIM37*. Triangles represent the mean for each biological replicate; coloured circles show individual data points from each of the replicates. Data acquired from $n = 3$ biological replicates, each with >40 cells. *P* values, unpaired two-tailed *t*-test. Mean ± s.e.m. **d**, A model illustrating the synthetic lethal effect of PLK4 inhibition with TRIM37 overexpression in 17q23-amplified breast cancer cells. MT, microtubule; Ub, ubiquitin.

(Extended Data Fig. 8a–c). As predicted, depletion of CEP192 sensitized these cells to centrosome loss (Fig. 3h). Treatment with 3MB-PP1 in CEP192-depleted RPE-1 cells also recapitulated the mitotic phenotypes we observed in acentrosomal MCF-7 cells, including a reduced frequency of non-centrosomal CEP192 foci, prolonged mitotic duration and a marked increase in mitotic errors (Fig. 3i, j, Extended Data Fig. 8d, e, Supplementary Videos 15–18). We conclude that TRIM37-dependent PCM depletion in mitosis leads to delayed and inefficient microtubule nucleation; these represent defects that can be exploited to induce mitotic catastrophe upon pharmacological depletion of centrosomes.

17q23-amplicon-positive breast cancer typically comprises highly proliferative, ER-positive luminal B-type tumours, characterized by high levels of genomic instability[4,5]. However, the mechanisms and driver genes that are responsible for genomic instability in 17q23-amplified tumours remain undefined. The high burden of genomic instability in MCF-7 cells drives their rapid genetic diversification in culture[29], which led us to consider the contribution of *TRIM37* overexpression to this process. Previous work has shown that delayed centrosome separation increases the rates of kinetochore mis-attachment and of mitotic errors in cancer cells[30–32]. We therefore investigated whether increased *TRIM37* expression during mitosis modulates the timing of centrosome maturation and separation. In contrast to RPE-1 cells, in which TRIM37 was transcriptionally downregulated in G2 phase and mitosis (Extended Data Fig. 9a–e), expression of TRIM37 protein persisted at high levels throughout the cell cycle in MCF-7 cells (Extended Data Fig. 9d). TRIM37 depletion in MCF-7 cells accelerated centrosome maturation by 20 min in late G2 phase (Extended Data Fig. 10a, d, Supplementary Videos 19, 20), and increased centrosome separation at mitotic entry (Extended Data Fig. 10b). Conversely, TRIM37 overexpression in RPE-1 cells delayed centrosome maturation in late G2 phase by 17 min (Extended Data Fig. 10c, e, Supplementary Videos 21, 22). Collectively, these data show that TRIM37-driven suppression of PCM assembly delays microtubule nucleation and centrosome separation in late G2 phase.

To test whether delays in centrosome separation at mitotic entry dependent on TRIM37 overexpression could cause mitotic errors, we compared the effect of the level of TRIM37 expression on the timing of centrosome separation, mitotic duration and the frequency of mitotic errors in 17q23-amplified (MCF-7 and MDA-MB-361) versus non-amplified (MDA-MB-231 and MDA-MB-436) breast cancer cell lines. TRIM37 depletion increased the distance between the centrosomes at early prophase and reduced mitotic duration in the 17q23-amplified cancer cell lines (Fig. 4a, c). By contrast, TRIM37 knockdown did not alter centrosome separation timing or mitotic duration in non-17q23-amplified breast cancer cells (Fig. 4a, c). Importantly, TRIM37 depletion also reduced the frequency of mitotic errors in 17q23-amplified breast cancer cells, but trended towards increasing the rate of cell division errors in non-17q23-amplified cancer cells (Fig. 4b). These data show that overexpression of TRIM37 delays the timing of centrosome separation at mitotic entry in 17q23-amplified breast cancer cells, and suggest that this delay in centrosome separation promotes genetic instability by increasing the frequency of mitotic errors.

We propose that TRIM37 usually acts to inhibit the assembly of non-centrosome-associated PCM into structures that would otherwise compromise mitotic fidelity. Consequently, the centrosomal defects that accompany *TRIM37* amplification may fuel the stochastic mitotic errors that contribute to the high burden of genomic instability in 17q23-amplified breast tumours and could drive tumour evolution. We also propose centrosome depletion as a therapeutic strategy to kill cancers that overexpress *TRIM37*. High levels of TRIM37 reduce the availability of PCM proteins, thereby impeding the formation of non-centrosomal PCM foci—assemblies that we propose are required for mitosis in the absence of centrosomes (Fig. 4d). Our work therefore indicates that the inhibition of PLK4, or other regulators of centrosome duplication or assembly, represents a promising strategy to selectively target breast cancers or other tumours[33] driven by 17q23 amplification.

Online content

Any methods, additional references, Nature Research reporting summaries, source data, extended data, supplementary information, acknowledgements, peer review information; details of author contributions and competing interests; and statements of data and code availability are available at https://doi.org/10.1038/s41586-020-2690-1.

1. Burrell, R. A., McGranahan, N., Bartek, J. & Swanton, C. The causes and consequences of genetic heterogeneity in cancer evolution. *Nature* **501**, 338–345 (2013).
2. Kalimutho, M. et al. Patterns of genomic instability in breast cancer. *Trends Pharmacol. Sci.* **40**, 198–211 (2019).
3. Lord, C. J. & Ashworth, A. PARP inhibitors: synthetic lethality in the clinic. *Science* **355**, 1152–1158 (2017).
4. Curtis, C. et al. The genomic and transcriptomic architecture of 2,000 breast tumours reveals novel subgroups. *Nature* **486**, 346–352 (2012).
5. Dawson, S.-J., Rueda, O. M., Aparicio, S. & Caldas, C. A new genome-driven integrated classification of breast cancer and its implications. *EMBO J.* **32**, 617–628 (2013).
6. Ali, H. R. et al. Genome-driven integrated classification of breast cancer validated in over 7,500 samples. *Genome Biol.* **15**, 431 (2014).
7. Wong, Y. L. et al. Reversible centriole depletion with an inhibitor of Polo-like kinase 4. *Science* **348**, 1155–1160 (2015).
8. Moyer, T. C., Clutario, K. M., Lambrus, B. G., Daggubati, V. & Holland, A. J. Binding of STIL to Plk4 activates kinase activity to promote centriole assembly. *J. Cell Biol.* **209**, 863–878 (2015).
9. Lambrus, B. G. et al. p53 protects against genome instability following centriole duplication failure. *J. Cell Biol.* **210**, 63–77 (2015).
10. Cuella-Martin, R. et al. 53BP1 integrates DNA Repair and p53-dependent cell fate decisions via distinct mechanisms. *Mol. Cell* **64**, 51–64 (2016).
11. Meitinger, F. et al. 53BP1 and USP28 mediate p53 activation and G1 arrest after centrosome loss or extended mitotic duration. *J. Cell Biol.* **214**, 155–166 (2016).
12. Fong, C. S. et al. 53BP1 and USP28 mediate p53-dependent cell cycle arrest in response to centrosome loss and prolonged mitosis. *eLife* **5**, e16270 (2016).
13. Lambrus, B. G. et al. A USP28–53BP1–p53–p21 signaling axis arrests growth after centrosome loss or prolonged mitosis. *J. Cell Biol.* **214**, 143–153 (2016).
14. Ciriello, G. et al. Comprehensive molecular portraits of invasive lobular breast cancer. *Cell* **163**, 506–519 (2015).
15. Pereira, B. et al. The somatic mutation profiles of 2,433 breast cancers refines their genomic and transcriptomic landscapes. *Nat. Commun.* **7**, 11479 (2016).
16. Monni, O. et al. Comprehensive copy number and gene expression profiling of the 17q23 amplicon in human breast cancer. *Proc. Natl Acad. Sci. USA* **98**, 5711–5716 (2001).
17. Pärssinen, J., Kuukasjärvi, T., Karhu, R. & Kallioniemi, A. High-level amplification at 17q23 leads to coordinated overexpression of multiple adjacent genes in breast cancer. *Br. J. Cancer* **96**, 1258–1264 (2007).
18. Sinclair, C. S., Rowley, M., Naderi, A. & Couch, F. J. The 17q23 amplicon and breast cancer. *Breast Cancer Res. Treat.* **78**, 313–322 (2003).
19. Balestra, F. R., Strnad, P., Flückiger, I. & Gönczy, P. Discovering regulators of centriole biogenesis through siRNA-based functional genomics in human cells. *Dev. Cell* **25**, 555–571 (2013).
20. Oegema, K., Davis, R. L., Lara-Gonzalez, P., Desai, A. & Shiau, A. K. CFI-400945 is not a selective cellular PLK4 inhibitor. *Proc. Natl Acad. Sci. USA* **115**, E10808 (2018).
21. Mason, J. M. et al. Functional characterization of CFI-400945, a Polo-like kinase 4 inhibitor, as a potential anticancer agent. *Cancer Cell* **26**, 163–176 (2014).
22. Kawakami, M. et al. Polo-like kinase 4 inhibition produces polyploidy and apoptotic death of lung cancers. *Proc. Natl Acad. Sci. USA* **115**, 1913–1918 (2018).
23. Bhatnagar, S. et al. TRIM37 is a new histone H2A ubiquitin ligase and breast cancer oncoprotein. *Nature* **516**, 116–120 (2014).
24. Branon, T. C. et al. Efficient proximity labeling in living cells and organisms with TurboID. *Nat. Biotechnol.* **36**, 880–887 (2018).
25. Roux, K. J., Kim, D. I., Raida, M. & Burke, B. A promiscuous biotin ligase fusion protein identifies proximal and interacting proteins in mammalian cells. *J. Cell Biol.* **196**, 801–810 (2012).
26. Oughtred, R. et al. The BioGRID interaction database: 2019 update. *Nucleic Acids Res.* **47**, D529–D541 (2019).
27. Wang, W., Xia, Z.-J., Farré, J.-C. & Subramani, S. TRIM37, a novel E3 ligase for PEX5-mediated peroxisomal matrix protein import. *J. Cell Biol.* **216**, 2843–2858 (2017).
28. Densham, R. M. et al. Human BRCA1–BARD1 ubiquitin ligase activity counteracts chromatin barriers to DNA resection. *Nat. Struct. Mol. Biol.* **23**, 647–655 (2016).
29. Ben-David, U. et al. Genetic and transcriptional evolution alters cancer cell line drug response. *Nature* **560**, 325–330 (2018).
30. Silkworth, W. T., Nardi, I. K., Paul, R., Mogilner, A. & Cimini, D. Timing of centrosome separation is important for accurate chromosome segregation. *Mol. Biol. Cell* **23**, 401–411 (2012).
31. Kaseda, K., McAinsh, A. D. & Cross, R. A. Dual pathway spindle assembly increases both the speed and the fidelity of mitosis. *Biol. Open* **1**, 12–18 (2012).
32. Zhang, Y. et al. USP44 regulates centrosome positioning to prevent aneuploidy and suppress tumorigenesis. *J. Clin. Invest.* **122**, 4362–4374 (2012).
33. Meitinger, F. et al. TRIM37 controls cancer-specific vulnerability to PLK4 inhibition. *Nature* https://doi.org/10.1038/s41586-020-2710-1 (2020).

Methods

No statistical methods were used to predetermine sample size. The experiments were not randomized and investigators were not blinded to allocation during experiments and outcome assessment.

Cell lines and culture conditions

MCF-7, MDA-MB-231, MDA-MB-436, DLD-1 and HCT-116 cells were grown in DMEM medium (Corning Cellgro) containing 10% fetal bovine serum (Sigma), 100 U/ml penicillin, 100 U/ml streptomycin and 2 mM L-glutamine. hTERT RPE-1 cells were grown in DMEM:F12 medium (Corning Cellgro) containing 10% fetal bovine serum (Sigma), 0.348% sodium bicarbonate, 100 U/ml penicillin, 100 U/ml streptomycin and 2 mM L-glutamine. MDA-MB-361 cells were grown in DMEM medium (ThermoFisher Scientific) containing 20% fetal bovine serum (Sigma), 100 U/ml penicillin, 100 U/ml streptomycin and 2 mM L-glutamine. BT474 and BT549 cells were grown in RPMI 1640 medium (ThermoFisher Scientific) containing 10% fetal bovine serum (Sigma), 100 U/ml penicillin, 100 U/ml streptomycin and 2 mM L-glutamine and 10 μg/ml bovine insulin (Sigma). All cell lines were maintained at 37 °C in a 5% CO_2 atmosphere with 21% oxygen and routinely checked for mycoplasma contamination.

Centrinone sensitivity in 3D tumour cell line and patient-derived organoid (PDO) cultures

Human breast tumour samples were obtained from adult female patients after informed consent as part of a non-interventional clinical trial (BTBC study REC no.: 13/LO/1248, IRAS ID 131133; principal investigator: A.N.J.T., study title: 'Analysis of functional immune cell stroma and malignant cell interactions in breast cancer in order to discover and develop diagnostics and therapies in breast cancer subtypes'). This study had local research ethics committee approval and was conducted adhering to the principles of the Declaration of Helsinki. Specimens were collected from surgery and transported immediately. A clinician histopathologist or pathology-trained technician identified and collected tumour material into basal culture medium. Tumour samples were coarsely minced with scalpels and then dissociated using a Gentle MACS dissociator (Miltenyi). The resulting cell suspension was mechanically disrupted, filtered and centrifuged. Resulting cell pellets were then plated into 3D cultures at approximately 1×10^3 to 2×10^3 cells per μl in Ocello PDX medium (OcellO B.V) and hydrogel as previously described[34–36]. All cultures were maintained in humidified incubators at 37 °C, 5% CO_2. For centrinone sensitivity analysis, PDOs (between passage 10 and 25) and tumour cell lines (short-tandem-repeat-typed every five passages to confirm identity) were dissociated to single-cell populations using TrypLE (Life Technologies). Cell suspensions were then dispensed into 384-well plates in Ocello PDX medium and hydrogel. Twenty-four h after seeding, cultures were treated with centrinone (diluted in 0.1% v/v DMSO) and then continuously cultured for a total of 13 d, with drug-containing medium being replenished every 4 d. After this point, cell viability was estimated using Cell Titer Glo 3D (CTG, Promega) as per the manufacturer's guidelines. CTG luminescence was measured using a Victor X5 plate reader (Perkin Elmer). Data are presented as per cent survival normalized to cells exposed to 0.1% v/v DMSO alone.

Gene targeting and stable cell lines

To generate CRISPR–Cas9-mediated knockout lines, gene-specific sgRNAs (*TP53Δ*, 5′-gtgcagctgtgggttgattc-3′; *TP53BP1Δ*, 5′-gaacgaggagacggtaatagt-3′; *USP28Δ*, 5′-tgccattgctttgagtctac-3′) were cloned into a modified pX330 vector (no. 42230; Addgene) containing a puromycin-resistance cassette. Cells were transiently transfected (Fugene HD, Promega) with the pX330 plasmids and positive selection of transfected cells was performed 2 d after transfection with 2.0 μg/ml puromycin. Monoclonal cell lines were isolated by limiting dilution. The presence of gene-disrupting insertions and deletions (indels) in edited cell lines was confirmed by Sanger sequencing, and the ablation of protein production was assessed by immunoblotting.

To generate EB1–TagRFP-, H2B–iRFP- and TagRFP–tubulin- or eGFP–tubulin-labelled cell lines, ORFs were cloned into FUGW lentiviral vectors. Fluorescent populations of cells were generated by lentivirus-mediated transduction. MCF-7 cells were transduced with H2B–iRFP and TagRFP–tubulin. RPE-1 cells were transduced with H2B–iRFP and eGFP–tubulin. DLD-1 cells expressing CEP192–mNeonGreen cells were transduced with H2B–iRFP and EB1–TagRFP. MDA-MB-361, MDA-MB-231 and MDA-MD-436 cells were transduced with H2B–iRFP. Polyclonal populations of cells expressing the desired fluorescent markers were used directly or isolated using FACS.

To generate EB3–mNeonGreen- and γ-tubulin–TagRFP-labelled cell lines, the two open reading frames (ORFs) separated by a T2A sequence were cloned into a CMV-puro lentiviral vector. RPE-1 cells were transduced with EB3–mNeonGreen and γ-tubulin–TagRFP dual-expressing lentivirus, and polyclonal populations of cells expressing both markers were selected using puromycin.

To generate *TRIM37*-overexpressing cell lines, the *TRIM37* ORF was cloned into a constitutive or tet-inducible lentiviral vector. The C18R and R67A mutations were introduced using PCR-directed mutagenesis and verified by Sanger sequencing. Cells were transduced and stable polyclonal populations of cells selected and maintained in the presence of 1.0 μg/ml puromycin.

To create the DLD-1 cell line expressing CEP192–mNeonGreen, an sgRNA targeting the *CEP192* translational stop codon (5′- cgactaattggtgaagctct-3′) was cloned into a pX459 vector (no. 62988; Addgene). To generate the CEP192 repair vector, we cloned a 2× mNeonGreen tag followed by a T2A-neomycin and a translational stop codon into a modified pUC vector. The 475-bp 5′ and 462-bp 3′ homology arms were PCR-amplified from genomic DLD-1 DNA and cloned on either side of the central 2× mNeonGreen-T2A-neomycin cassette. DLD-1 cells were transiently transfected (X-tremeGENE HP, Roche) with the pX459 plasmid and repair vector. Selection of transfected cells was performed 5 d after transfection with 400 μg/ml G418.

RNA interference

shRNAs targeting *TRIM37* (*TRIM37*-1, 5′-tcgagaatatgatgctgtg-3′; *TRIM37*-2, 5′-aggactttgctggaggtta-3′) were cloned into the pGIPz (Thermofisher Scientific) vector. shRNAs targeting *CEP192* (*CEP192*-1, 5′-cctgttacataaaccagagat-3′; *CEP192*-2, 5′-gaggcatcagttaatactgat-3′) were cloned into pLKO.1. Stable shRNA-mediated knockdown cell lines were generated by lentivirus-mediated transduction. Polyclonal populations of cells were subsequently selected and maintained in the presence of puromycin (1.0 μg/ml). Knockdown efficiency was assessed by immunoblotting.

Lentiviral production and transduction

Lentiviral expression vectors were cotransfected into 293FT cells with the lentiviral packaging plasmids psPAX2 and pMD2.G (Addgene no. 12260 and no. 12259). In brief, 3×10^6 293FT cells were seeded into a poly-L-lysine-coated 10-cm culture dish the day before transfection. For each 10-cm dish, the following DNA was diluted in 0.6 ml of OptiMEM (Thermo Fisher Scientific): Four and half μg of lentiviral vector, 6 μg of psPAX2 and 1.5 μg of pMD2.G. Separately, 72 μl of 1 μg/μl 25 kDa polyethylenimine (PEI; Sigma) was diluted into 1.2 ml of OptiMEM, briefly vortexed and incubated at room temperature for 5 min. After incubation, the DNA and PEI mixtures were combined, briefly vortexed and incubated at room temperature for 20 min. During this incubation, the culture medium was replaced with 17 ml of pre-warmed DMEM + 1% FBS. The transfection mixture was then added drop-wise to the 10-cm dish. Viral particles were collected 48 h after the medium change and filtered through a 0.45-μm PVDF syringe filter. The filtered supernatant was either concentrated in 100-kDa Amicon Ultra Centrifugal Filter Units (Millipore) or used directly to infect cells. Aliquots were snap-frozen

and stored at −80 °C. For transduction, lentiviral particles were diluted in complete growth medium supplemented with 10 μg/ml polybrene (Sigma) and added to cells.

Chemical inhibitors

3MB-PP1 (Millipore) was dissolved in DMSO and used at a final concentration of 10 μM, and centrinone (a gift from K. Oegema) was dissolved in DMSO and used at a final concentration of 125 nM, unless otherwise indicated. CFI-400945 (Cayman Chemicals) was dissolved in DMSO and used at a final concentration of 50 or 500 nM. ZM447439 (Cayman Chemicals) was dissolved in DMSO and used at a final concentration of 2 μM. MG132 (Sigma) was dissolved in DMSO and used at a final concentration of 10 μM. CHX (VWR International) was dissolved in DMSO and used at a final concentration of 100 μg/ml. RO-3306 (Sigma) was dissolved in DMSO and used at a final concentration of 9 μM.

TRIM37 RNA abundance in PDOs

RNA from PDO cell pellets was extracted using the RNeasy kit (Qiagen) according to the manufacturer's instructions. Quality and quantity of RNA were assessed using a Qubit and Bioanalyzer (Agilent). NEBNEXT Ultra II Directional RNA and polyA RNA selection kits (Illumina) were used to generate paired-end sequencing libraries that were sequenced on an Illumina NovaSeq 6000 S2 platform. Paired-end reads were aligned to the human reference genome GRCh38 using STAR v.2.5.1b[37] using quantMode GeneCounts and twopassMode basic alignment settings. Feature quantification was performed using GENCODE (v.22) GTF file. Post alignment quality control was performed using RseQC (v.2.6.3)[38]. Data was normalized using the TMM method (trimmed mean of *M*-values) of edgeR[39] and *TRIM37* mRNA expression values converted into *Z* scores adjusted to the median of all mRNA species in the sample.

BioID sample preparation, mass spectrometry and data analysis

To generate cell lines for BioID, puro-sensitive RPE-1 cells were transduced with lentivirus containing tet-inducible miniTurbo control, or miniTurbo-TRIM37 constructs. Forty-eight h after transduction, cells were selected in 2.5 μg/ml puromycin for 2 d. Cells were then expanded into 7 × 15-cm dishes. One day before biotin labelling, 1 μg/ml doxycycline was added to induce expression of miniTurbo constructs. Twenty-four h after the start of induction, with cells at about 60% confluency, 10 μM dimethylenastron (Sigma) was added to cell culture medium to block cells in mitosis. After 2 h of mitotic block, medium was supplemented with 250 uM D-biotin (P212121; prepared as 250 mM stock in DMSO) to initiate labelling of proximity interactors. After 4 h of biotin labelling, mitotic samples were collected by mitotic shake-off, and the remaining interphase cells were collected by scraping. All samples were transferred to 15-ml conical flasks and rinsed 4 times with PBS to remove excess biotin. Cell pellets were lysed in approximately 1.5 ml lysis buffer (all buffer recipes have previously been published[40]) by gentle pipetting followed by sonication. Lysates were clarified by centrifugation at 16,000*g* for 10 min at 4 °C. To enrich for biotinylated material, 60 μl of streptavidin agarose bead resin (Pierce) was washed with lysis buffer, then incubated with clarified lysates, rotating at 4 °C, overnight. Samples were then washed for 10 min each with a series of 4 wash buffers that decreased in detergent concentration. Beads were then washed a final two times in × PBS, left in about 60 μl volume PBS, then frozen until ready for analysis by the mass spectrometry facility.

In preparation for mass spectrometry, proteins were reduced with 1.75 μl 15 mg/ml DTT in 10 mM TEAB, shaking at 56 °C for 50 min. Samples were then cooled to room temperature, the pH adjusted to 8 with 500 mM TEAB buffer, and alkylated with 1.8 μl 36 mg/ml iodoacetomide in 100 mM TEAB for 20 min at room temperature, in the dark. Next, 20 ng/μl trypsin (Promega) was added to proteolyze the samples at 37 °C, overnight. Supernatant was collected, and the beads were washed with 0.1× TFA 3 times, with washes added to supernatant. The pH was adjusted to acidic range, and peptides desalted on u-HLB Oasis plates, eluted with 60% acetonitrile/0.1% TFA, and dried. Ten per cent desalted peptides were analysed on a Nano LC-MS/MS instrument on Q Exactive Plus (Thermo) in FTFT mode. Tandem mass spectrometry data were searched with Mascot via PD2.2 against RefSeq2017_83 human species database and a small enzyme and standard (BSA)-containing database using the FilesRC option, with mass tolerance of 3 ppm on precursors and 0.01 Da on fragments, and annotating variable modifications such as oxidation on M, carbamidomethyl C, deamidation NQ, with and without biotin K. The Mascot .dat files were (1) compiled in Scaffold and (2) processed in PD2.2 to identify peptides and proteins using Percolator as a PSM validator.

Protein hits identified only in miniTurbo-TRIM37 BioID, and hits with spectral counts in miniTurbo-TRIM37 BioID that were twofold greater than those of mTurbo alone were considered as candidates for TRIM37 interaction. The filtered list of BioID hits was annotated with Gene Ontology (GO) terms via the Panther classification system[41] and analysed using the statistical overrepresentation test (binomial) to derive *P* values[42].

Antibody techniques

For immunoblot analyses, protein samples were separated by SDS–PAGE, transferred onto nitrocellulose membranes with a Trans-Blot Turbo Transfer System (BioRad) and then probed with the following primary antibodies: YL1/2 (rat anti-α-tubulin, ThermoFisher Scientific, MA1-80017, 1:3,000), TRIM37 (rabbit, Bethyl, A301-174A, 1:1,000), p53 (mouse, Dako, M7001, 1:1,000), β-actin (mouse, Sigma, A1978, 1:1,000), HA-11 (mouse, BioLegend, 901501, 1:1,000), GST (mouse, Sigma, G1160, 1:1,000), CEP192 (rabbit, home-made, 1:1,000), CDK5RAP2 (rabbit, Millipore, 06-1398, 1:2,500), pericentrin (rabbit, Abcam, ab4448, 1:2,500), cyclin A (mouse, SantaCruz Biotechnology, sc-53228, 1:1,000), phosphorylated histone H3 (rabbit, Millipore, 06-570, 1:2,000). Proteins were then detected using HRP-conjugated anti-mouse (goat, ThermoFisher Scientific, 31432, 1:1,000) or anti-rabbit (goat, ThermoFisher Scientific, 31462, 1:10000) secondary antibodies and enhanced chemiluminescence (Clarity, Bio-Rad). Signals were visualized and acquired using the Gel DocXRSystem (Bio-Rad).

For immunofluorescence, cells were grown on 18-mm glass coverslips and fixed for 10 min in either 4% formaldehyde at room temperature, or 100% ice-cold methanol at −20 °C for 10 min. Cells were blocked in 2.5% FBS, 200 mM glycine, and 0.1% Triton X-100 in PBS for 1 h. Antibody incubations were conducted in the blocking solution for 1 h. DNA was stained with DAPI and cells were mounted in ProLong Gold Antifade (Invitrogen). Staining was performed with the following primary antibodies: centrin (mouse, Millipore, 04-1624, 1:1,000), CDK5RAP2 (rabbit, Millipore, 06-1398, 1:2,500), γ-tubulin–Cy5 (directly labelled goat, raised against the following peptide: CDEYHAATRPDYISWGTQEQ, this study, 1:1,000), pericentrin (rabbit, Abcam, ab4448, 1:2,500), CEP192–Cy5 (directly labelled goat, raised against CEP192 amino acids 1–211, this study, 1:1,000), YL1/2 (rat anti-α-tubulin, ThermoFisher Scientific, MA1-80017, 1:3,000), EB1 (mouse, Santa Cruz, sc-47704, 1:200).

Immunofluorescence images were collected using a Deltavision Elite system (GE Healthcare) controlling a Scientific CMOS camera (pco. edge 5.5). Acquisition parameters were controlled by SoftWoRx suite (GE Healthcare). Images were collected at room temperature (25 °C) using an Olympus 40× 1.35 NA, 60× 1.42 NA or Olympus 100× 1.4 NA oil objective at 0.2-μm *z*-sections. Images were acquired using Applied Precision immersion oil ($N = 1.516$). For quantification of signal intensity at the centrosome, deconvolved 2D maximum intensity projections were saved as 16-bit TIFF images. Signal intensity was determined using ImageJ by drawing a circular region of interest (ROI) around the centriole (ROI S). A larger concentric circle (ROI L) was drawn around ROI S. ROI S (S) and ROI L (L) were transferred to the channel of interest and the signal in ROI S was calculated using the formula $I_S - [(I_L - I_S/A_L - A_S) \times A_S]$, in which *A* is area and *I* is integrated pixel intensity.

To measure the distance between two centrosomes in prophase, cells were fixed in 4% formaldehyde at room temperature for 10 min. Coverslips were blocked and stained as above with the following primary antibodies: CENP-F (sheep, a gift from S. Taylor, 1:2,000), phospho-histone H3 (mouse, Cell Signaling, 9701, 1:2,000), and CEP192 (rabbit, a gift from K. Oegema, this study, 1:2,000). Phospho-histone-H3-positive cells with a nuclear-envelope-localized CENP-F signal were selected for analysis. The distance between two centrosomes was measured from 3D-image stacks using Imaris (Bitplane) software.

Live cell microscopy

Fluorescent cell lines were seeded into either 4-chamber, 35-mm glass-bottom culture dishes (Greiner) or 4-well chamber slides (Ibidi) and maintained at 37 °C in an environmental control station. Long-term time-lapse imaging was performed using a Deltavision Elite system (GE Healthcare) controlling a Scientific CMOS camera (pco.edge 5.5.). Images were acquired with an Olympus 40× 1.4 NA oil objective. Every 5 min, 7 × 3-µm *z*-sections were acquired in respective fluorescent channels and by differential inference contrast. Time-lapse imaging of PCM foci and EB1 or EB3 comets was performed using a Lecia SP-8 confocal microscope, equipped with a resonance scanner, and 405-nm, 488-nm, 552-nm and 638-nm laser lines. Images were acquired with a Leica 40×1.3 NA or 63×1.4 NA oil objectives. For time-lapse imaging of PCM foci, images were captured every 5 min in 20 × 1-µm *z*-sections. For time-lapse imaging of EB1 or EB3 comets, images were collected every 2 s in a single *z*-plane. Movies were deconvolved using the LIGHTNING adaptive approach, and assembled and analysed in FIJI. Mitotic duration was calculated as the time taken from nuclear envelope breakdown to the onset of anaphase.

Microtubule regrowth assay

Cells were treated with 3.3 µM nocodazole for 1 h to disrupt the microtubule network, then quickly rinsed 3× with warmed medium (37 °C) to remove the drug. Cells were then incubated in warmed medium for 90 s to allow microtubule regrowth, fixed in 100% ice-cold methanol for 10 min, and processed as described in 'Antibody techniques' for immunofluorescence. For fluorescence intensity quantification, images were analysed in ImageJ using a circular area of 5 µm to quantify α-tubulin and EB1 signals around centrosomes. Background fluorescence using a circle of corresponding size was subtracted from each measurement.

PLK4i survival assays

For short-term survival assays, cells seeded in triplicate at 1.25×10^4 cells per well in 6-well plates were treated with either DMSO control or PLK4i (10 µM 3MB-PP1, or 125 nM centrinone) 16 h later. After the indicated number of days, cells were fixed and stained using 0.5% (w/v) crystal violet in 20% (v/v) methanol for 5 min. Excess of reagent was extensively washed with distilled water and plates dried overnight. For quantification, bound crystal violet was dissolved in 10% (v/v) acetic acid in dH_2O and absorbance of 1:50 dilutions were measured at 595 nm in a WPA S800 Spectrawave spectrophotometer (Biochrom). Optical density at 595 nm was measured as a quantitative metric of relative growth.

For long-term clonogenic survival assays, 500 cells were seeded in a 10-cm^2 culture dish in triplicate and left to adhere overnight. Cells were treated the next day and left to grow for about 14 d or until colonies were visible by eye. Plates were then stained with crystal violet dye (Sigma) and colonies counted. The relative colony growth was assessed relative to DMSO control plates.

RNA extraction and reverse-transcription qPCR

Total RNA was extracted using the RNeasy Plus Mini kit (Qiagen) and reverse transcription was performed using the iScript cDNA Synthesis Kit (Bio-Rad) following manufacturer's protocol. *TRIM37* transcripts were measured by qPCR in triplicate on a CFX96 Real-Time Analyzer (Bio-Rad) using Quantifast SYBR Green reagent (QIAGEN), normalized to reference gene *SMG9* and quantified using the $\Delta\Delta C_t$ method to obtain relative expression. Thermocycling conditions were set as follows: 1 cycle (95 °C for 5 mins), 40 cycles (95 °C for 15 s, 58 °C for 60 s). Primer sequences were *TRIM37* forward (5′-TCAGCTGTATTAGGCGCTGG-3′), *TRIM37* reverse (5′-ACTTCTTCTGCCCAACGACA-3′), *SMG9* forward (5′- GCCCTGGAGAAGAATGAA-3′) and *SMG9* reverse (5′-GGTGAAA GACAACAGCATC-3′).

Flow cytometry

G0/G1, S and G2/M cell cycle profiles were assessed using 5′-bromouridine (BrdU) incorporation and propidium iodide (PI) staining. Cells were pulsed with 10 µM BrdU (Sigma-Aldrich) for 30 min, trypsinized and washed with 1% BSA in PBS (1,500 rpm, 5 min) before being fixed in 70% ethanol. DNA denaturation was performed using a solution of 0.2 mg/ml of pepsin (Sigma-Aldrich) in 2 M HCl for 20 min at room temperature. Cells were washed twice with PBS and re-suspended in a solution containing anti-BrdU–FITC-conjugated antibody (rat, Bio-Rad, MCA2060FT, 1:100) in 0.5% (v/v) Tween-20, 0.5% (v/v) BSA in PBS and incubated for 1 h in the dark. For determination of the mitotic phase cell population (M), cells fixed in 70% ethanol were permeabilized with 0.2% Tween-20 in 2 M HCl for 10 min. Cells were then stained with anti-phosphorylated histone H3 (Ser10) antibody (mouse, Cell Signaling Technology, 9706, 1:50) in 1% (v/v) BSA in PBS for 3 h. Cells were then washed twice with PBS, re-suspended in a solution containing anti-mouse Alexa-Fluor-488-conjugated antibody (goat, ThermoFisher Scientific, A-11029, 1:250) in 1% (v/v) BSA in PBS and incubated for 1 h in the dark. For total DNA staining, including those used for determination of sub-G1 population and ploidy analyses, a 20-min incubation at 37 °C in a solution of PI/RNaseA (10 µg/ml and 0.1 mg/ml, respectively) in PBS was performed. Samples were analysed using an Attune NxT flow cytometer (Life Technologies) and data processing was done using FlowJo software.

SA-β-gal staining

The SA-β-gal activity of DMSO- or centrinone-treated MCF-7 cells was assessed using a staining kit (Cell Signaling, no. 9860), as per the manufacturer's protocol. Stained cells were imaged with a Nikon wide-field TE2000U Microscope at 200× magnification. For quantification, up to 200 cells per condition were counted across multiple fields to determine the percentage of SA-β-gal-positive cells.

Reporting summary

Further information on research design is available in the Nature Research Reporting Summary linked to this paper.

Data availability

Data that support the findings of this study are available from the corresponding authors upon reasonable request. Source data are provided with the paper.

34. Di, Z. et al. Ultra high content image analysis and phenotype profiling of 3D cultured micro-tissues. *PLoS ONE* **9**, e109688 (2014).
35. Booij, T. H. et al. Development of a 3D tissue culture-based high-content screening platform that uses phenotypic profiling to discriminate selective inhibitors of receptor tyrosine kinases. *J. Biomol. Screen.* **21**, 912–922 (2016).
36. Sandercock, A. M. et al. Identification of anti-tumour biologics using primary tumour models, 3-D phenotypic screening and image-based multi-parametric profiling. *Mol. Cancer* **14**, 147 (2015).
37. Dobin, A. et al. STAR: ultrafast universal RNA-seq aligner. *Bioinformatics* **29**, 15–21 (2013).
38. Wang, L., Wang, S. & Li, W. RSeQC: quality control of RNA-seq experiments. *Bioinformatics* **28**, 2184–2185 (2012).
39. Robinson, M. D., McCarthy, D. J. & Smyth, G. K. edgeR: a Bioconductor package for differential expression analysis of digital gene expression data. *Bioinformatics* **26**, 139–140 (2010).
40. Firat-Karalar, E. N. & Stearns, T. in *Methods in Cell Biology* **vol. 129** (eds Basto, R. & Oegema, K.) 153–170 (Academic, 2015).

41. Mi, H. et al. PANTHER version 11: expanded annotation data from Gene Ontology and Reactome pathways, and data analysis tool enhancements. *Nucleic Acids Res.* **45**, D183–D189 (2017).
42. Mi, H., Muruganujan, A., Casagrande, J. T. & Thomas, P. D. Large-scale gene function analysis with the PANTHER classification system. *Nat. Protocols* **8**, 1551–1566 (2013).

Acknowledgements This work was supported by a Cancer Research UK Career Development Fellowship C52690/A19270 (to J.R.C.), and by National Institutes of Health grants R01GM114119 and R01GM133897, an American Cancer Society Scholar grant RSG-16-156-01-CCG, and an American Cancer Society Mission Boost Grant MBG-19-173-01-MBG (to A.J.H.). Z.Y.Y. is supported by the National Science Scholarship from A*STAR, Singapore. J.R.C. holds a Lister Institute Research Prize Fellowship. The Wellcome Centre for Human Genetics is supported by Wellcome grant 090532/Z/09/Z. The C.J.L. and A.N.J.T laboratories are funded by NC3Rs (NC/P001262/1), Breast Cancer Now funding to the Breast Cancer Now Toby Robins Research Centre (CTR-Q4-Y2), private donations to the ICR Development Office, and NHS funding to the NIHR Biomedical Research Centres at Guy's and St Thomas' NHS Foundation Trust and King's College London, and the Royal Marsden Hospital. We also thank R. Peat for breast cancer cell lines.

Author contributions Z.Y.Y. and B.G.L. designed, performed and analysed the majority of the experiments, and prepared the figures. M.-A.D., D.M. and C.M.G. assisted with associated cytogenetic experiments. K.H.Z. performed and analysed centrosomal intensity quantification experiments. L.T.E. generated the cell lines and analysed the movies for the data in Fig. 4b, c. P.M.S. created and performed the imaging of the DLD-1 cell line that expresses CEP192–mNeonGreen. T.P. analysed centrosome separation in 17q23-amplified and non-17q23-amplified cell lines. E.P. created the *PLK4*^{AS} *TP53*$^{-/-}$ RPE-1 cells that express EB3–mNeonGreen, TUBG1–TagRFP and H2B–iRFP. L.A.R. analysed PCM foci in mitotic MDA-MB-436 and DLD-1 cells. R.M., E.G.K., L.M.B., D.N. and S.H. conducted and analysed 3D tumour cell line and PDO experiments, under the supervision of A.N.J.T. and C.J.L. J.R.C. and A.J.H. conceived and co-supervised the study, designed experiments, and analysed the data. Z.Y.Y., B.G.L., J.R.C. and A.J.H. co-wrote the manuscript.

Competing interests C.J.L. received research funding from AstraZeneca, Merck KGaA and Artios; received consultancy, SAB membership or honoraria payments from Syncona, Sun Pharma, Gerson Lehrman Group, Merck KGaA, Vertex, AstraZeneca, Tango, 3rd Rock, Ono Pharma and Artios; and has stock in Tango and Ovibio. None of these is directly relevant to the work published and/or discussed in this Article. C.J.L. is also a named inventor on patents describing the use of DNA repair inhibitors and stands to gain from the development as part of the ICR Rewards to Inventors scheme. A.N.J.T received research funding from AstraZeneca and Merck KGaA that is not directly relevant to work published or discussed in this Article. A.N.J.T. also receives payments from the ICR Rewards to Inventors scheme associated with patents describing the use of DNA repair inhibitors and stands to gain from their development.

Additional information

Supplementary information is available for this paper at https://doi.org/10.1038/s41586-020-2690-1.

Correspondence and requests for materials should be addressed to J.R.C. or A.J.H.

Peer review information *Nature* thanks Renata Basto, Sarah McClelland and the other, anonymous, reviewer(s) for their contribution to the peer review of this work.

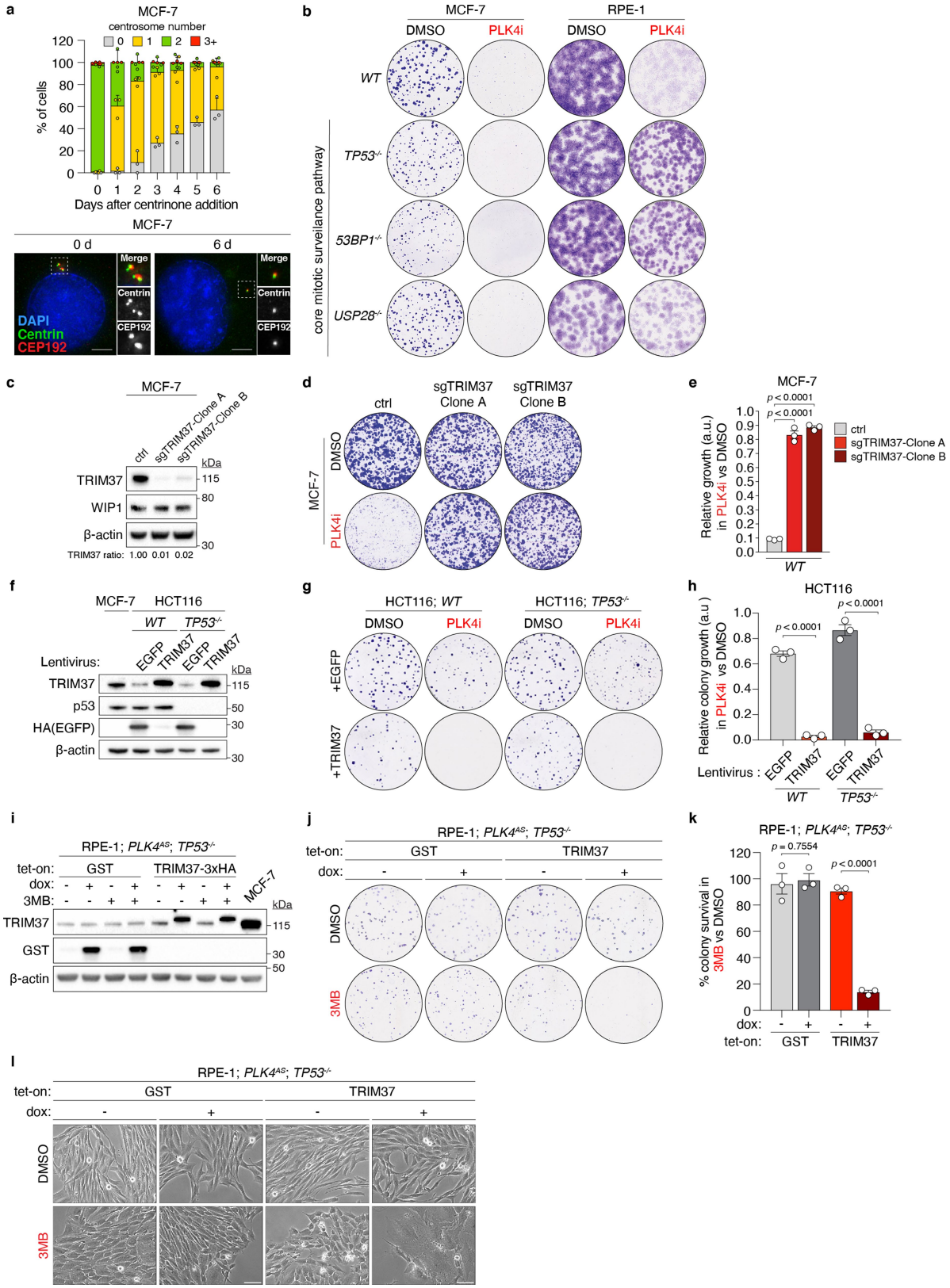

Extended Data Fig. 1 | See next page for caption.

Extended Data Fig. 1 | TRIM37 overexpression in HCT116 and RPE-1 cells recapitulates synthetic lethality with centrosome loss. Related to Fig. 1. **a**, Top, centrosome number distribution in interphase MCF-7 cells at various times after addition of centrinone (PLK4i) (125 nM). Mean ± s.e.m. Bottom, representative images of centrosome staining (centrioles labelled by centrin, and PCM labelled by CEP192). $n = 3$ biological replicates, each comprising >100 cells. **b**, Representative data of a 14-day clonogenic survival assay of MCF-7 and RPE-1 cells with the indicated genotypes treated with DMSO (control) or centrinone (PLK4i) (125 nM). $n = 3$ biological replicates. **c**, Immunoblot showing TRIM37 protein levels in two WT MCF-7 clones stably expressing control vector or a *TRIM37*-targeting sgRNA. β-Actin, loading control. Representative data; $n = 3$ biological replicates. For gel source data, see Supplementary Fig. 1. **d**, Representative data of a 10-day clonogenic survival of indicated MCF-7 cell lines treated with DMSO (control) or centrinone (PLK4i) (125 nM). **e**, Quantification of $n = 3$ biological replicates in **d**. *P* values, unpaired two-tailed *t*-test. Mean ± s.e.m. **f**, Immunoblot of lysates prepared from WT and $TP53^{-/-}$ HCT116 cells expressing a control (*eGFP*) or *TRIM37* transgene. MCF-7 cells were used as a reference for TRIM37 protein overexpression in a 17q23-amplified cell line. β-Actin, loading control. Representative data; $n = 3$ biological replicates. For gel source data, see Supplementary Fig. 1. **g**, Representative data of a 14-day clonogenic survival assay of HCT116 cells treated with DMSO (control) or centrinone (PLK4i) (125 nM). **h**, Quantification of $n = 3$ biological replicates in **g**. *P* values, unpaired two-tailed *t*-test. Mean ± s.e.m. **i**, Immunoblot showing doxycycline-induced *GST* or *TRIM37* expression in $PLK4^{AS}$ $TP53^{-/-}$ RPE-1 cells. β-Actin, loading control. Representative data; $n = 3$ biological replicates. For gel source data, see Supplementary Fig. 1. **j**, Representative data of a 14-day colony survival assay of $PLK4^{AS}$ $TP53^{-/-}$ RPE-1 cells expressing doxycycline-inducible *GST* (control) or *TRIM37* transgenes, treated with DMSO (control) or 3MB-PP1 (3MB). AS, analogue sensitive. **k**, Quantification of $n = 3$ biological replicates in **j**. *P* values, unpaired two-tailed *t*-test. Mean ± s.e.m. **l**, Representative images of $PLK4^{AS}$ $TP53^{-/-}$ RPE-1 cells in **j**. Scale bars, 100 µm.

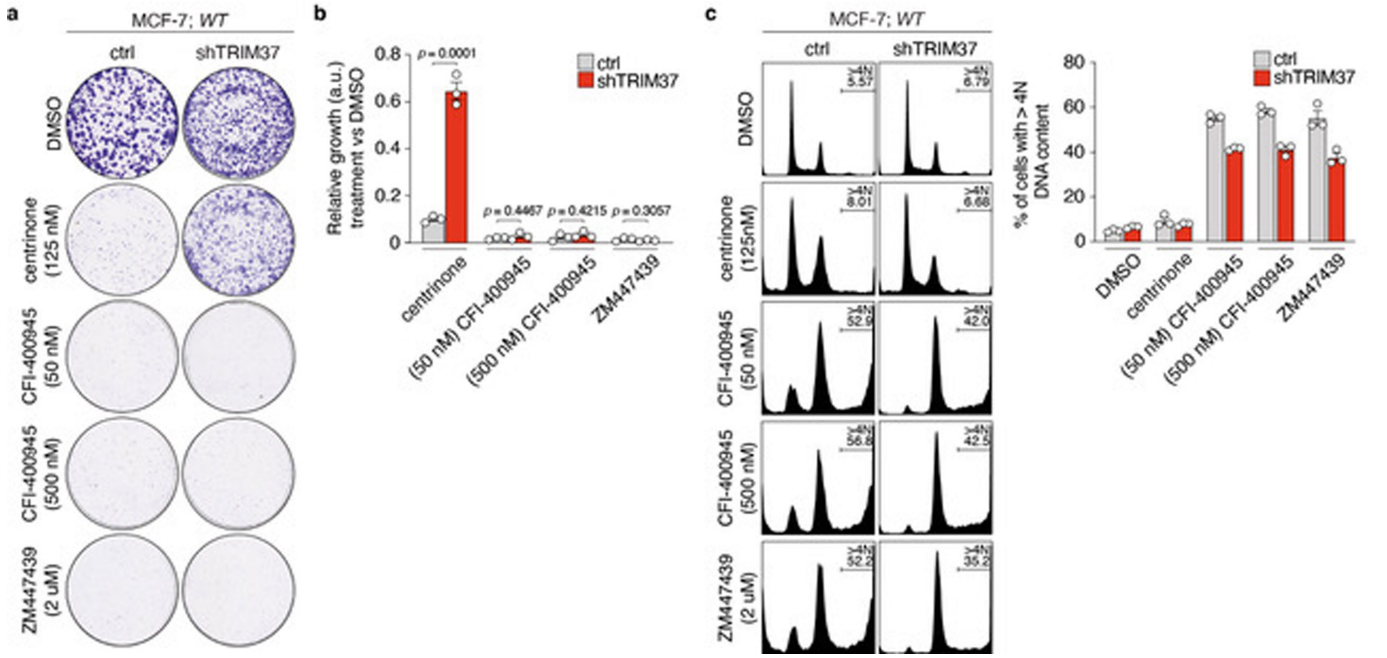

Extended Data Fig. 2 | Inhibitor selectivity for PLK4—and not other kinases—is required for the synthetic lethal killing of cells overexpressing TRIM37. a, Representative data of a 10-day clonogenic survival of indicated MCF-7 cell lines treated with DMSO (control), centrinone, CFI-400945 or ZM447439. Data acquired in parallel to experiment in Fig. 1c, d. **b**, Quantification of **a**, $n = 3$ biological replicates. *P* values, unpaired two-tailed *t*-test. Mean ± s.e.m. **c**, Left, representative flow cytometric analysis of DNA content in MCF-7 cells treated with DMSO (control), centrinone, CFI-400945 or ZM447439 for 3 d. Right, quantification of the percentage of cells with >4N DNA content (polyploidy). $n = 3$ biological replicates. Mean ± s.e.m.

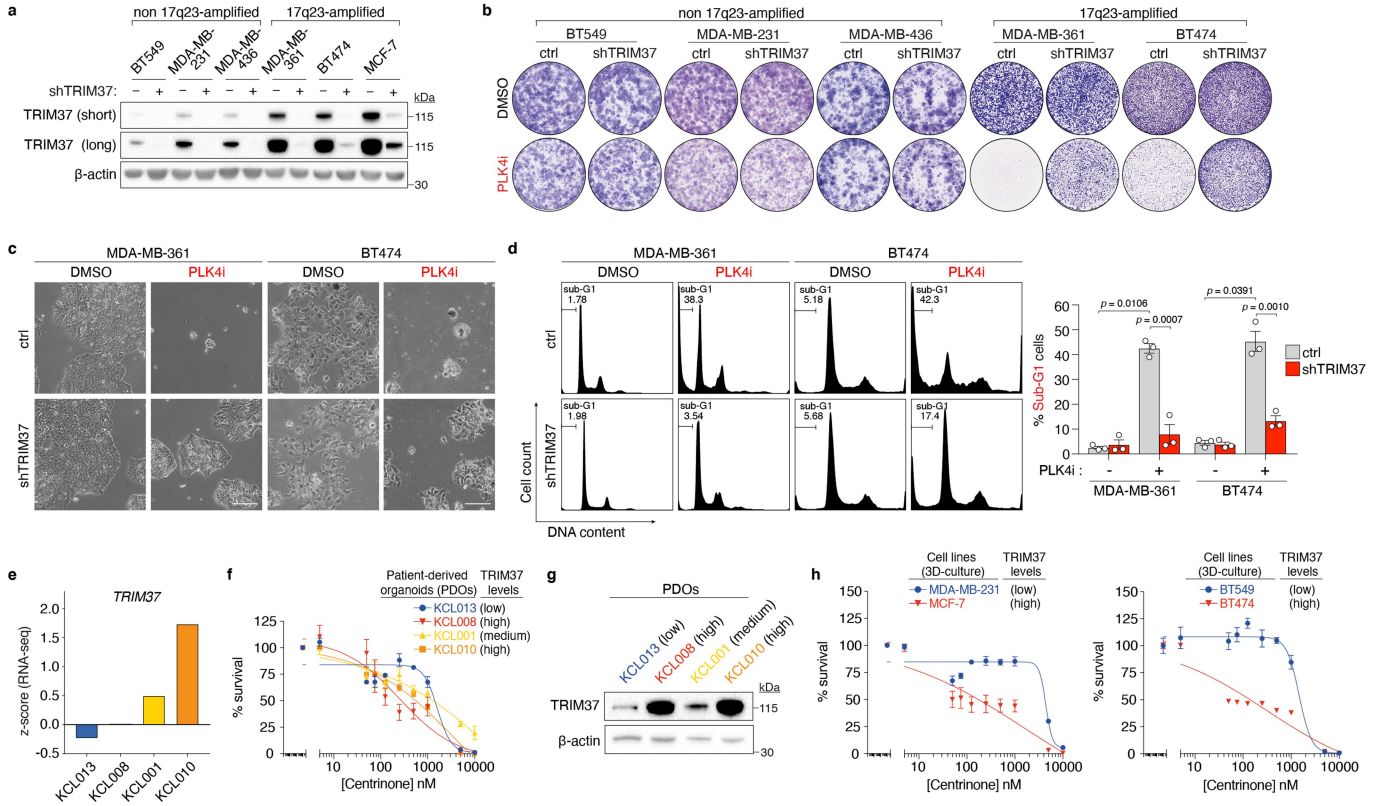

Extended Data Fig. 3 | Additional characterization of TRIM37 expression and synthetic lethality in breast cancer cell lines and patient-derived organoids (PDOs). Related to Fig. 1. **a**, Immunoblot showing TRIM37 protein levels in the indicated 17q23-amplified cell lines (MDA-MB-361, BT474 and MCF-7) and non-17q23-amplified cell lines (BT549, MDA-MB-231 and MDA-MB-436) expressing control or *TRIM37*-targeting shRNA. β-Actin, loading control. Representative data; $n = 3$ biological replicates. For gel source data, see Supplementary Fig. 1. **b**, Clonogenic survival of 17q23-amplified and non-17q23-amplified cell lines treated with DMSO (control) or centrinone (PLK4i) (125 nM). Representative data; $n = 3$ biological replicates. **c**, Images of DMSO- or PLK4i-treated MDA-MB-361 and BT474 cells expressing control vector or *TRIM37*-targeting shRNA. Scale bars, 200 µm. Representative data; $n = 3$ biological replicates. **d**, Left, Representative flow cytometric DNA content analysis in DMSO- or PLK4i-treated MDA-MB-361 and BT474 cells. Percentages of sub-G1 events are indicated. Right, percentage of sub-G1 cells across $n = 3$ biological replicates. *P* values, unpaired two-tailed *t*-test. Mean ± s.e.m. **e**, *TRIM37* gene expression in PDOs. Gene expression is reported as a *z*-score derived from RNA-seq data sets across $n = 22$ independent biological samples. **f**, Viability of patient-derived breast tumour organoids following a 14-d exposure to the indicated concentrations of centrinone. Data from $n = 2$ biological replicates are shown. Mean ± s.e.m. **g**, Immunoblot showing TRIM37 protein levels in PDOs. β-Actin, loading control. Data from $n = 1$ biological replicate. For gel source data, see Supplementary Fig. 1. **h**, Viability of 3D cultures of the indicated cell lines following a 14-d exposure to the indicated concentrations of centrinone. Left, $n = 2$ biological replicates, Mean ± s.e.m. Right, $n = 4$ technical replicates, Mean ± s.e.m.

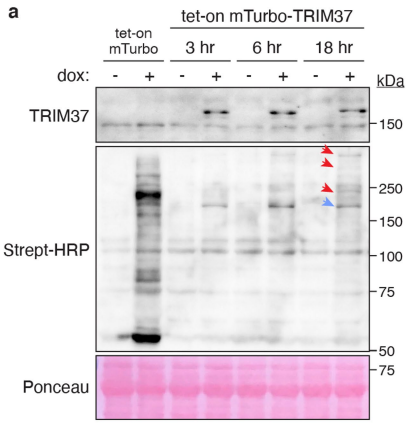

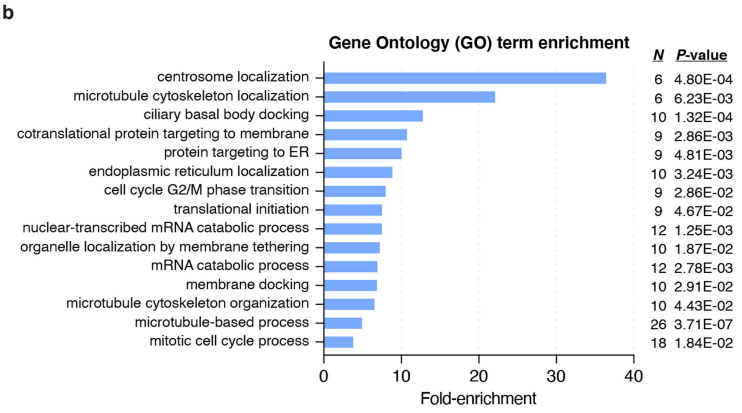

c

Rank	Gene Symbol	ctrl int.	ctrl mit.	TRIM37 int.	TRIM37 mit.	
1	CEP170	15	24	142	76	●
2	TRIM37	0	0	115	66	●
3	LRP1	7	0	52	21	
4	TJP1	0	0	52	13	
5	NCOR2	0	1	41	5	
6	CEP350	3	4	28	17	●
7	MAP4	0	0	31	19	●
8	XRN1	0	2	23	19	
9	CEP192	0	0	29	5	●
10	JMJD1C	0	1	28	2	
11	SIPA1L3	2	2	25	4	
12	EDC3	2	4	5	10	
13	TNRC6B	0	1	20	7	
14	ARHGAP29	1	2	14	4	●
15	ZNF281	3	0	12	7	
16	SF3B3	0	0	12	8	
17	NCOR1	0	0	19	2	
18	CNBP	3	1	7	7	
19	SNW1	0	0	1	10	
20	CEP152	0	0	13	3	●
21	SPATA2	1	4	3	9	●
22	LDLR	0	1	5	10	
23	MT2A	0	3	3	12	
24	HSPA8	2	2	6	6	
25	PCCB	2	0	8	3	
26	HRNR	0	1	1	7	
27	FBN1	0	0	8	5	
28	NOTCH2	0	0	3	8	
29	ALB	0	0	0	13	
30	PCM1	1	0	10	3	●

● centrosomal protein
● TRIM37 self-tagging

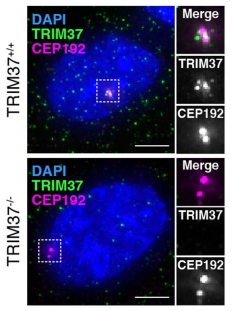

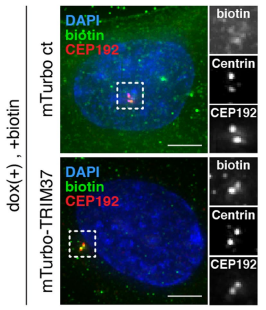

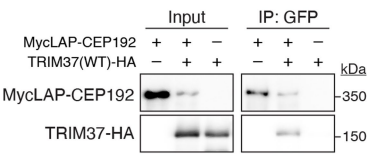

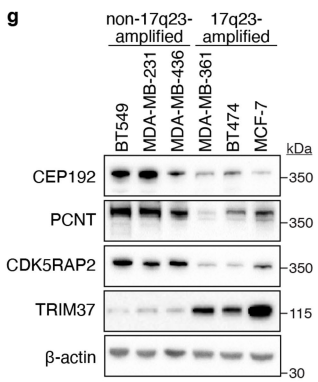

Extended Data Fig. 4 | See next page for caption.

Extended Data Fig. 4 | TRIM37 localizes to centrosomes, where it interacts with, and regulates the abundance of PCM proteins. Related to Fig. 3. **a**, Immunoblot showing TRIM37 and biotinylated proximity interactors. Ponceau-stained blot indicates loading. Data are from a single experiment performed in duplicate. For gel source data, see Supplementary Fig. 1. **b**, Gene ontology analysis of mass spectrometry data. **c**, Thresholded mass spectrometry results displaying the top 30 proximity interactors by spectral count. Interactors were filtered to isolate those with >2 × more peptides in the mTurbo-TRIM37 sample compared to control. **d**, Left, immunofluorescence of TRIM37 in *TRIM37*$^{+/+}$ and *TRIM37*$^{-/-}$ RPE-1 cells. Scale bars, 5 µm. Right, quantification of TRIM37 intensity at the centrosome in RPE-1 cells. $n = 3$ biological replicates, each comprising >40 cells. *P* values, unpaired two-tailed *t*-test. Mean ± s.e.m. **e**, Immunofluorescence of biotin-labelled proteins in mTurbo cell lines. Representative data; $n = 3$ biological replicates. Scale bars, 5 µm. **f**, Co-immunoprecipitation showing the interaction of TRIM37 with CEP192. Representative data; $n = 3$ biological replicates. For gel source data, see Supplementary Fig. 1. **g**, Immunoblot showing the levels of TRIM37 and PCM components in non-17q23-amplified versus 17q23-amplified cell lines. β-Actin, loading control. Representative data; $n = 3$ biological replicates. For gel source data, see Supplementary Fig. 1.

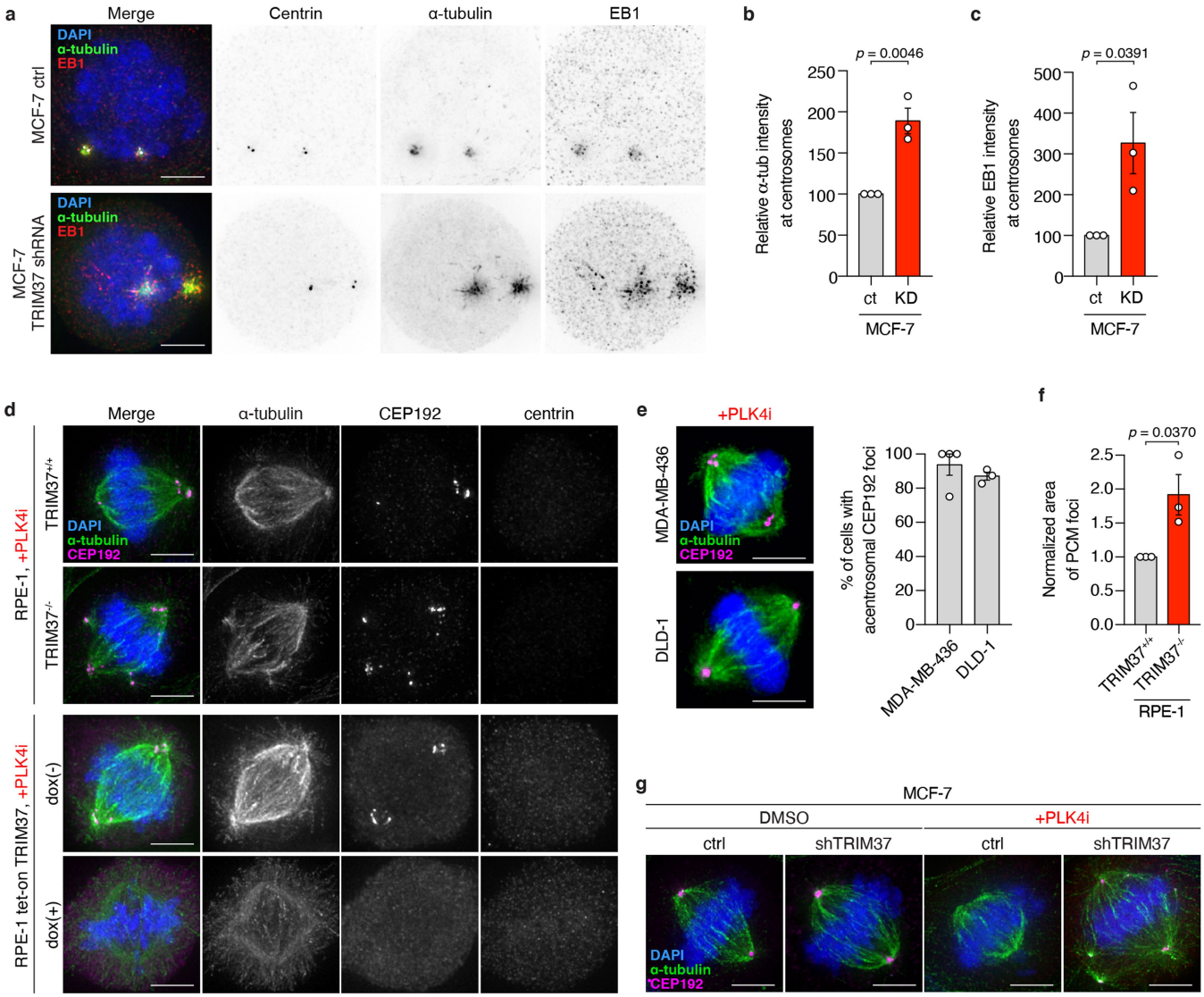

Extended Data Fig. 5 | TRIM37 suppresses microtubule nucleation by the centrosome and supresses the formation of non-centrosomal PCM foci. Related to Fig. 3. **a**, Microtubule regrowth following nocodazole washout in control vector- or *TRIM37*-shRNA-expressing MCF-7 mitotic cells. Representative images from **b**. $n = 3$ biological replicates. Scale bars, 5 µm. **b**, Quantification of microtubule regrowth following nocodazole washout in control vector- or *TRIM37*-shRNA-expressing MCF-7 mitotic cells. $n = 3$ biological replicates, each with >25 cells. *P* values, unpaired two-tailed *t*-test. Mean ± s.e.m. **c**, Quantification of centrosomal EB1 intensity following nocodazole washout in control vector- or *TRIM37*-shRNA-expressing MCF-7 mitotic cells. $n = 3$ biological replicates, each with >25 cells. *P* values, unpaired two-tailed *t*-test. Mean ± s.e.m. **d**, Representative images of mitotic PCM foci in acentrosomal RPE-1 cells described in Fig. 3d. $n = 3$ biological replicates. Scale bars, 5 µm. **e**, Left, representative images of mitotic PCM foci in acentrosomal MDA-MB-436 and DLD-1 cells. Scale bars, 5 µm. Right, quantification of mitotic PCM foci in centrinone-treated MDA-MB-436 and DLD-1 cells that lacked centrosomes. $n \geq 3$ biological replicates, each comprising ≥ 84 cells for DLD-1 cells and ≥ 6 cells for MDA-MB-436 cells. Mean ± s.e.m. **f**, Quantification of CEP192 foci area in *TRIM37*$^{+/+}$ versus *TRIM37*$^{-/-}$ RPE-1 cells in **d**. $n = 3$ biological replicates, each comprising >20 cells. *P* values, unpaired two-tailed *t*-test. Mean ± s.e.m. **g**, Representative images for spindle length analysis in indicated MCF-7 cells described in Fig. 3g. $n = 3$ biological replicates. Scale bars, 5 µm.

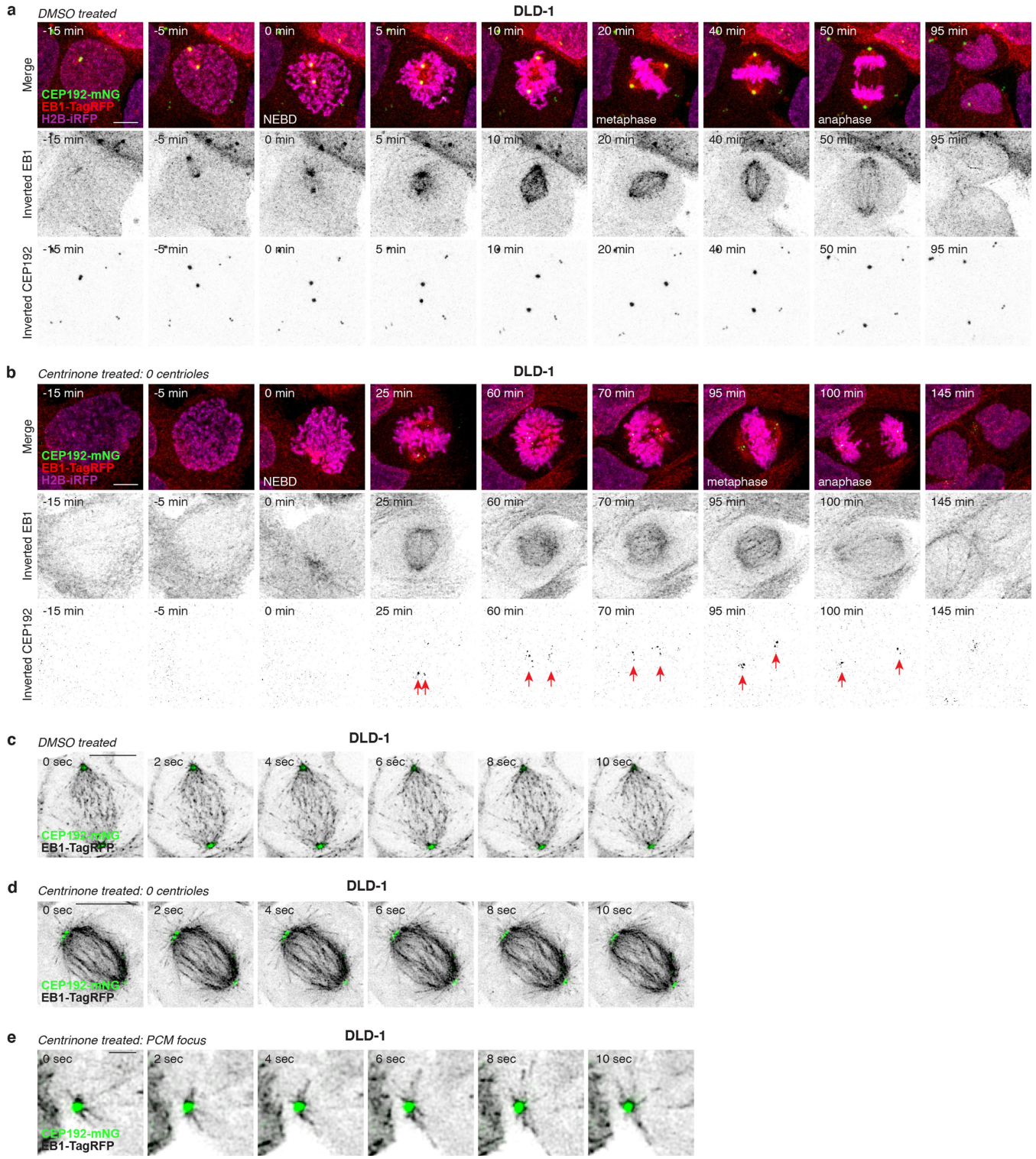

Extended Data Fig. 6 | Non-centrosomal PCM foci nucleate microtubules and contribute to spindle assembly in DLD-1 cells. Related to Fig. 3. **a**, Representative time-lapse images of mitosis in DMSO-treated control DLD-1 cells. $n = 3$ biological replicates. Scale bar, 5 µm. **b**, Representative time-lapse images of PCM foci formation during mitosis in acentrosomal DLD-1 cells. Scale bar, 5 µm. $n = 3$ biological replicates. Arrows indicate PCM foci. **c**, Representative time-lapse images of microtubule nucleation from centrosomes in the mitotic spindle of DMSO-treated control DLD-1 cells. $n = 3$ biological replicates. Scale bar, 5 µm. **d**, Representative time-lapse images of microtubule nucleation from PCM foci incorporated into the mitotic spindle of acentrosomal DLD-1 cells. $n = 3$ biological replicates. Scale bar, 5 µm. **e**, Representative time-lapse images of microtubule nucleation from a PCM focus before its incorporation into the mitotic spindle of the acentrosomal cell shown in **d**. $n = 3$ biological replicates. Scale bar, 1 µm.

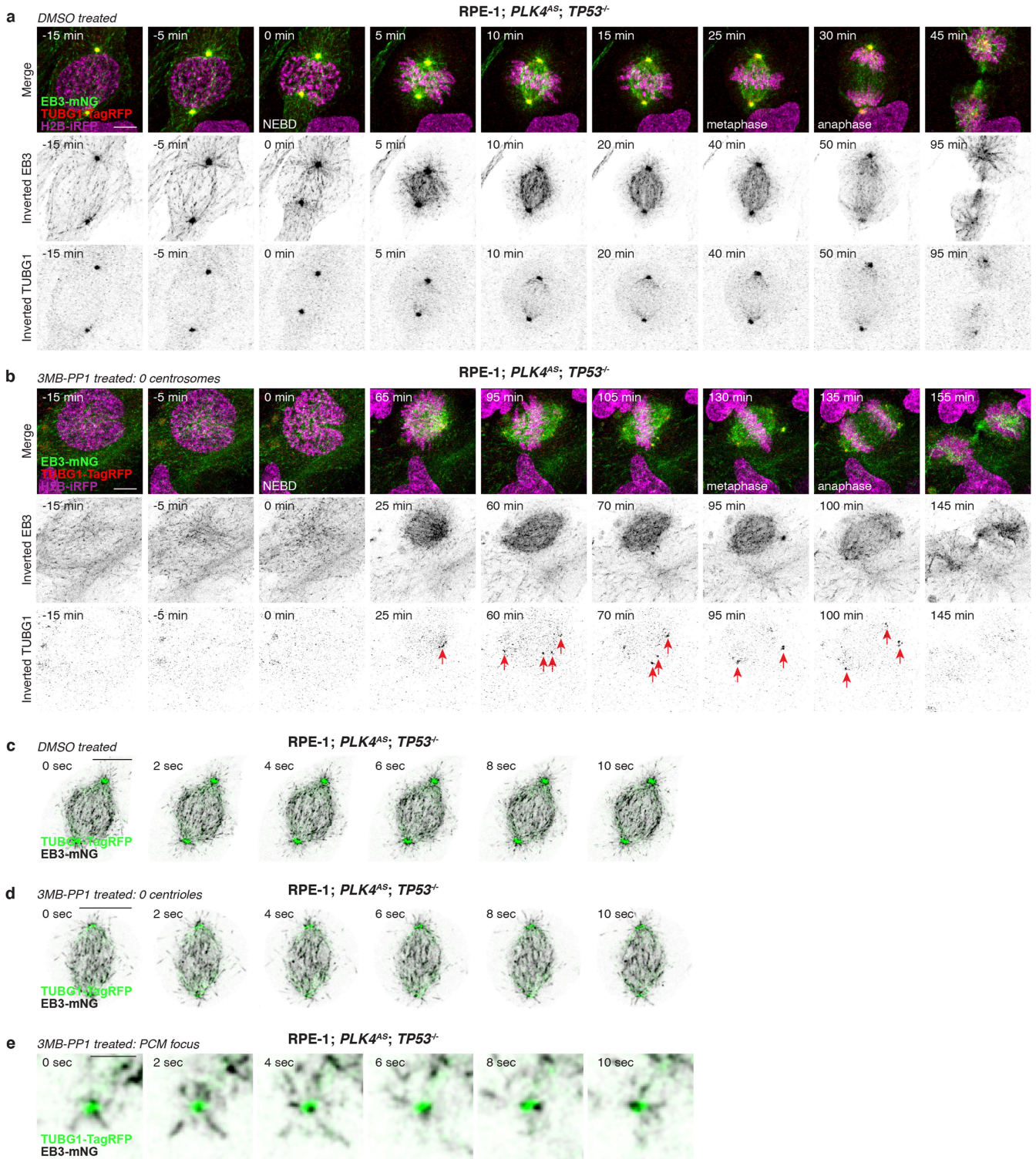

Extended Data Fig. 7 | Non-centrosomal PCM foci nucleate microtubules and contribute to spindle assembly in RPE-1 cells. Related to Fig. 3. **a**, Representative time-lapse images of mitosis in DMSO-treated control *PLK4*^{AS} *TP53*$^{-/-}$ RPE-1 cells. $n = 3$ biological replicates. Scale bar, 5 µm. **b**, Representative time-lapse images of PCM foci formation during mitosis in acentrosomal *PLK4*^{AS} *TP53*$^{-/-}$ RPE-1 cells. $n = 3$ biological replicates. Scale bar, 5 µm. Arrows indicate PCM foci. **c**, Representative time-lapse images of microtubule nucleation from centrosomes in the mitotic spindle of DMSO-treated control *PLK4*^{AS} *TP53*$^{-/-}$ RPE-1 cells. $n = 3$ biological replicates. Scale bars, 5 µm. **d**, Representative time-lapse images of microtubule nucleation from PCM foci incorporated into the mitotic spindle of acentrosomal *PLK4*^{AS} *TP53*$^{-/-}$ RPE-1 cells. $n = 3$ biological replicates. Scale bar, 5 µm. **e**, Representative time-lapse images of microtubule nucleation from a PCM focus before its incorporation into the mitotic spindle in acentrosomal *PLK4*^{AS} *TP53*$^{-/-}$ RPE-1. $n = 3$ biological replicates. Scale bar, 1 µm.

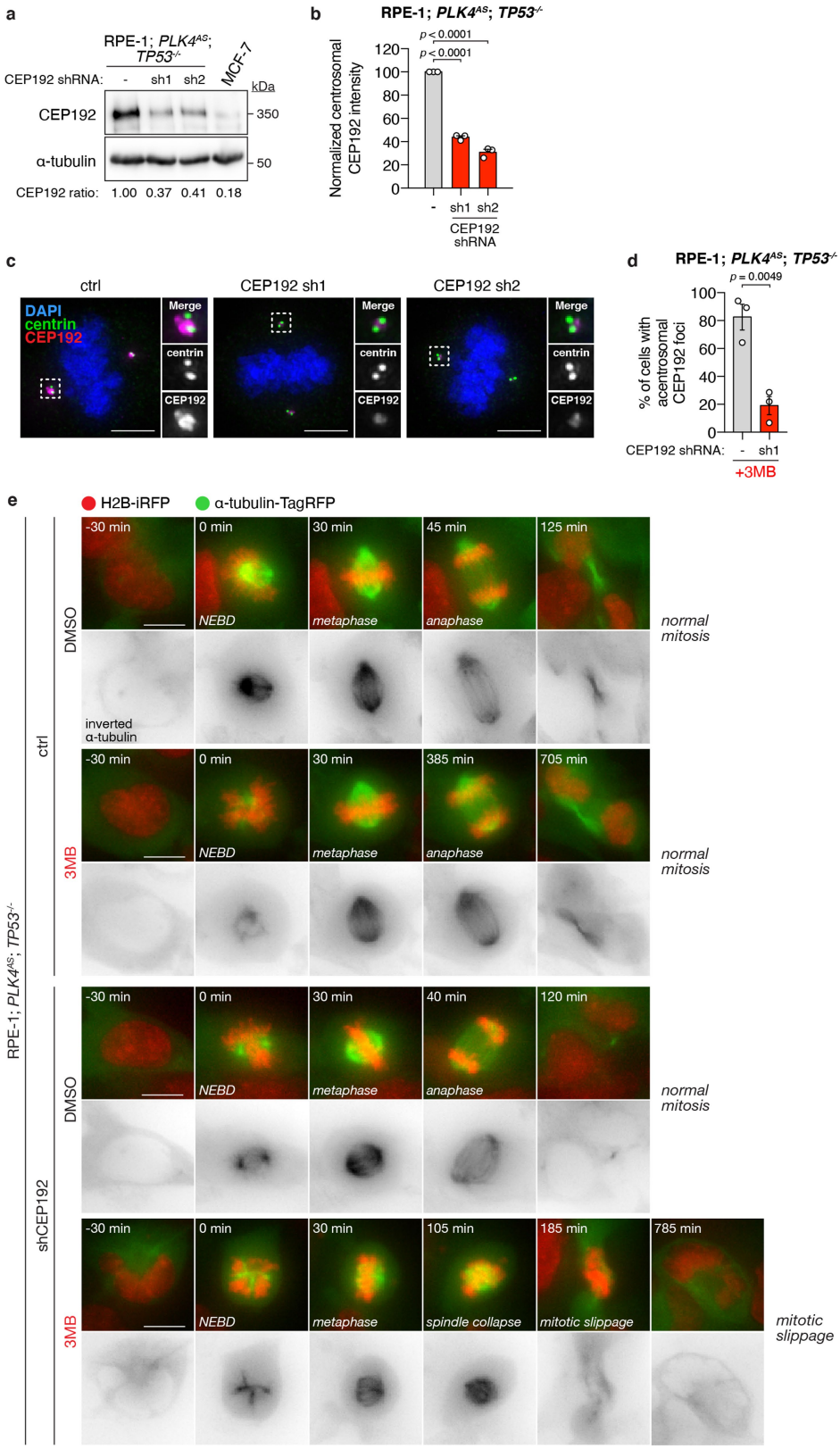

Extended Data Fig. 8 | Depletion of CEP192 in RPE-1 cells recapitulates the synthetic lethal mitotic phenotypes observed in high-TRIM37 expressing cells. Related to Fig. 3. **a**, Immunoblot showing the CEP192 levels in indicated control and CEP192-depleted *PLK4*^{AS} *TP53*$^{-/-}$ RPE-1 cells. α-Tubulin, loading control. For gel source data, see Supplementary Fig. 1. **b**, Quantification of mitotic centrosomal CEP192 signal in the same cells as described in **a**. $n = 3$ biological replicates, each comprising >30 cells. *P* values, unpaired two-tailed *t*-test. Mean ± s.e.m. **c**, Representative images of centrosomal CEP192 in the same cells as described in **a**. Scale bars, 5 µm. **d**, Quantification of the percentage of 3MB-PP1 (3MB)-treated *PLK4*^{AS} *TP53*$^{-/-}$ RPE-1 cells with acentrosomal mitotic CEP192 PCM foci. $n = 3$ biological replicates, each comprising >30 cells. *P* values, unpaired two-tailed *t*-test. Mean ± s.e.m. **e**, Representative time-lapse images of mitotic progression in DMSO- or 3MB-PP1 (3MB)-treated control and CEP192-depleted *PLK4*^{AS} *TP53*$^{-/-}$ RPE-1 cells. Cells are labelled with H2B-iRFP and tagRFP-tubulin. $n = 3$ biological replicates.

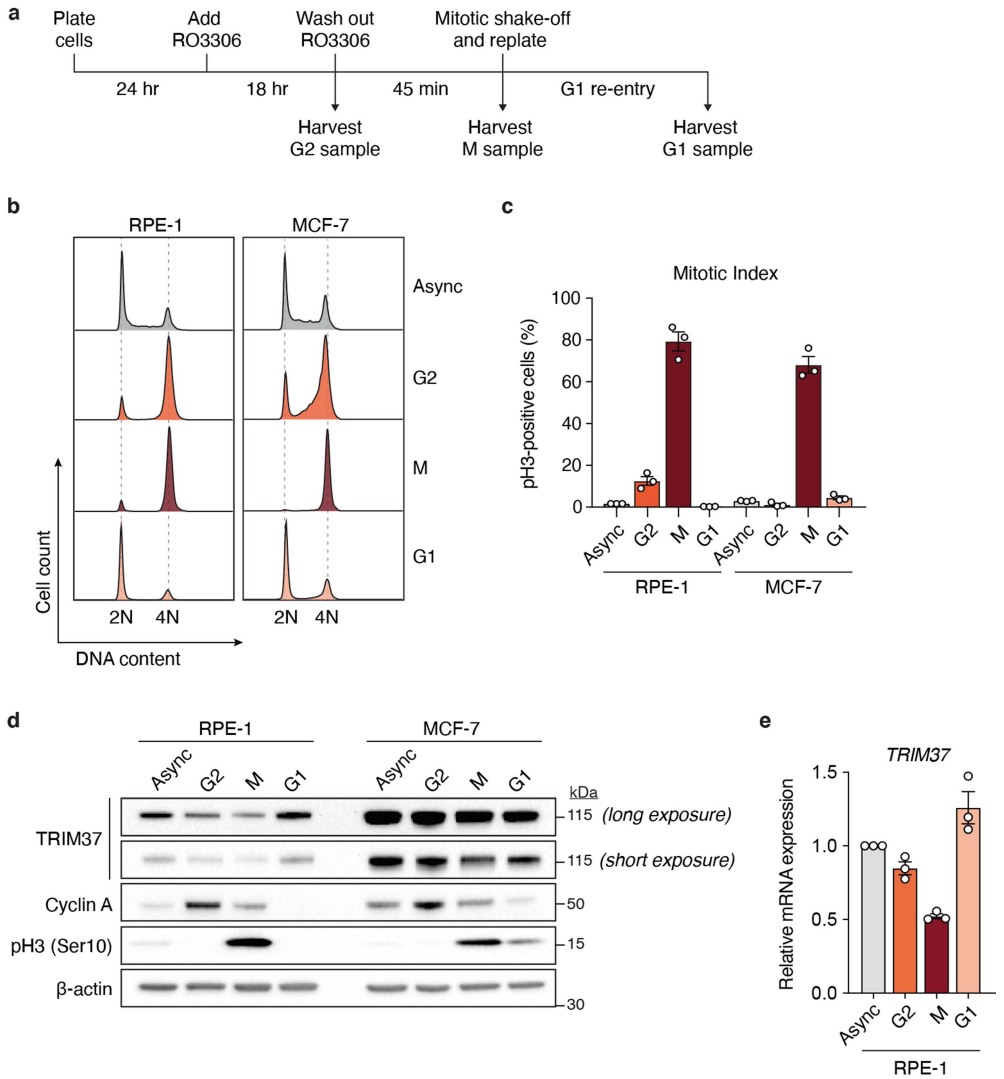

Extended Data Fig. 9 | Cell cycle regulation of *TRIM37* expression. Related to Fig. 4. **a**, Schematic of the experimental protocol used for cell cycle synchronization. Samples were subjected to dual flow cytometry staining of phospho-histone Ser10 (pH3) to mark mitotic cells and propidium iodide (PI) to determine synchronization efficiency. M, mitotic phase. **b**, Flow cytometric DNA content analysis of samples collected according to **a**. Left, RPE-1. Right, MCF-7. Async, asynchronous. **c**, Mitotic index of cell cycle samples as determined by the percentage of pH3-positive cells with 4N DNA content. $n = 3$ biological replicates. Mean ± s.e.m. **d**, Immunoblot showing endogenous TRIM37, cyclin A and pH3 in samples analysed in **b**. β-Actin, loading control. For gel source data, see Supplementary Fig. 1. **e**, RT-qPCR analysis indicating relative *TRIM37* mRNA expression in RPE-1 cells analysed in **b**. Data were normalized to *TRIM37* mRNA expression in asynchronous cells. $n = 3$ biological replicates. Mean ± s.e.m.

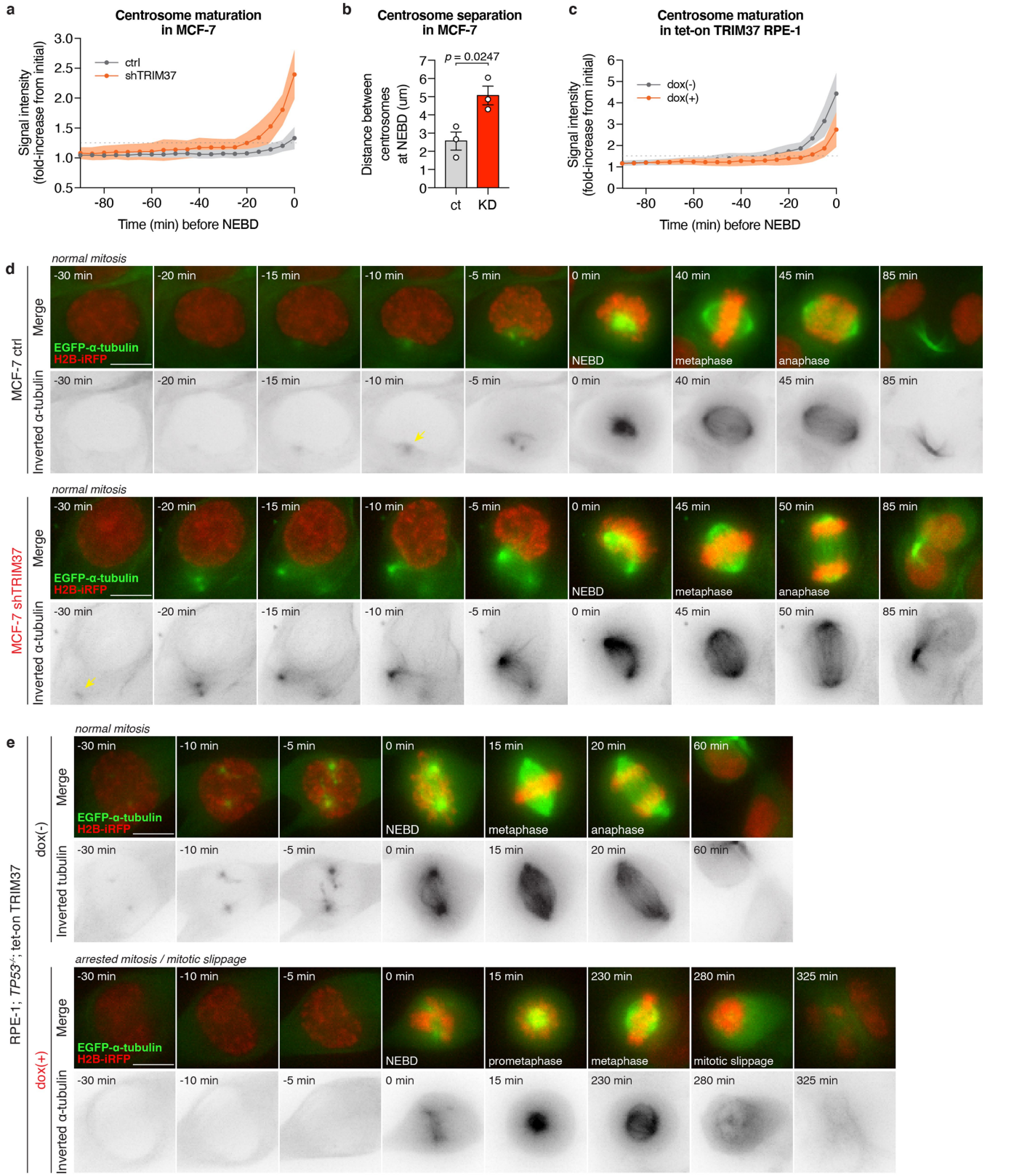

Extended Data Fig. 10 | TRIM37 overexpression delays centrosome maturation in G2/M phase. Related to Fig. 4. **a**, Quantification of centrosomal α-tubulin intensity from time-lapse movies of dividing MCF-7 cells expressing either control vector or *TRIM37*-targeting shRNA. Quantification of >20 cells. Mean ± s.e.m. **b**, Quantification of the distance between the two centrosomes at NEBD in MCF-7 cells. $n = 3$ biological replicates, each comprising >12 cells. *P* values, unpaired two-tailed *t*-test. Mean ± s.e.m. **c**, Quantification of centrosomal α-tubulin intensity from time-lapse movies of dividing RPE-1 tet-on TRIM37 cells. Quantification of >20 cells. Mean ± s.e.m. **d**, Representative time-lapse images of centrosome maturation in MCF-7 cells. $n = 3$ biological replicates. Scale bars, 5 µm. **e**, Representative time-lapse images of centrosome maturation in RPE-1 tet-on TRIM37 cells. $n = 3$ biological replicates. Scale bars, 5 µm.

Corresponding author(s): J. Ross Chapman, Ph.D
Andrew J. Holland, Ph.D

Last updated by author(s): May 6, 2020

Reporting Summary

Nature Research wishes to improve the reproducibility of the work that we publish. This form provides structure for consistency and transparency in reporting. For further information on Nature Research policies, see Authors & Referees and the Editorial Policy Checklist.

Statistics

For all statistical analyses, confirm that the following items are present in the figure legend, table legend, main text, or Methods section.

n/a	Confirmed
☐	☒ The exact sample size (*n*) for each experimental group/condition, given as a discrete number and unit of measurement
☐	☒ A statement on whether measurements were taken from distinct samples or whether the same sample was measured repeatedly
☐	☒ The statistical test(s) used AND whether they are one- or two-sided *Only common tests should be described solely by name; describe more complex techniques in the Methods section.*
☒	☐ A description of all covariates tested
☐	☒ A description of any assumptions or corrections, such as tests of normality and adjustment for multiple comparisons
☐	☒ A full description of the statistical parameters including central tendency (e.g. means) or other basic estimates (e.g. regression coefficient) AND variation (e.g. standard deviation) or associated estimates of uncertainty (e.g. confidence intervals)
☒	☐ For null hypothesis testing, the test statistic (e.g. *F*, *t*, *r*) with confidence intervals, effect sizes, degrees of freedom and *P* value noted *Give P values as exact values whenever suitable.*
☒	☐ For Bayesian analysis, information on the choice of priors and Markov chain Monte Carlo settings
☒	☐ For hierarchical and complex designs, identification of the appropriate level for tests and full reporting of outcomes
☒	☐ Estimates of effect sizes (e.g. Cohen's *d*, Pearson's *r*), indicating how they were calculated

Our web collection on statistics for biologists contains articles on many of the points above.

Software and code

Policy information about availability of computer code

Data collection	Gel/membrane Imaging: Image Lab v5.2.1; Flow cytometry: Attune NxT Software V2.5; RT-PCR: Bio-Rad CFX Manager™ Software Immunofluorescence: GE Healthcare Deltavision Elite system and SoftWoRx suite or Leica Microsystems and LAS X elements.
Data analysis	FlowJo v10; GraphPad Prism v7 was typically used for all presented statistical analyses; Image analysis was preformed using FIJI or Imaris v9.2.1 (Bitplane).

For manuscripts utilizing custom algorithms or software that are central to the research but not yet described in published literature, software must be made available to editors/reviewers. We strongly encourage code deposition in a community repository (e.g. GitHub). See the Nature Research guidelines for submitting code & software for further information.

Data

Policy information about availability of data

All manuscripts must include a data availability statement. This statement should provide the following information, where applicable:

- Accession codes, unique identifiers, or web links for publicly available datasets
- A list of figures that have associated raw data
- A description of any restrictions on data availability

All source data for graphs and gels in Fig. 1–4 and Extended Data Fig. 1–10 are available as .xslx tables and Supplementary Information within the manuscript. Other data that support the findings of this study are available from the corresponding authors upon reasonable request.

Field-specific reporting

Please select the one below that is the best fit for your research. If you are not sure, read the appropriate sections before making your selection.

☒ Life sciences ☐ Behavioural & social sciences ☐ Ecological, evolutionary & environmental sciences

For a reference copy of the document with all sections, see nature.com/documents/nr-reporting-summary-flat.pdf

Life sciences study design

All studies must disclose on these points even when the disclosure is negative.

Sample size	No statistical methods were used to predetermine the experimental sample size. All experiments conducted with cell lines were performed with multiple biological replicates based on previous experience with the sample size required to identify statistically significant effect sizes.
Data exclusions	No data were excluded from the analyses.
Replication	Following extensive optimization, biological experiments were typically performed in 3 biological replicates (each performed identically on different days) with consistent results. In the some cases, each biological replicate (e.g. clonogenic assay, flow cytometric sample) involved 2-3 technical replicates. Attempts to replicate findings were successful for all of the experiments presented in the manuscript.
Randomization	Experiments were performed using populations of manipulated cell lines and therefore randomization was not appropriate.
Blinding	Investigators were not blinded to the experimental conditions used during most experiments. The data reported are not subjective but rather based on quantitative analysis of phenotypes such as cell survival, distance, mitotic time and error frequency.

Reporting for specific materials, systems and methods

We require information from authors about some types of materials, experimental systems and methods used in many studies. Here, indicate whether each material, system or method listed is relevant to your study. If you are not sure if a list item applies to your research, read the appropriate section before selecting a response.

Materials & experimental systems

n/a	Involved in the study
☐	☒ Antibodies
☐	☒ Eukaryotic cell lines
☒	☐ Palaeontology
☒	☐ Animals and other organisms
☐	☒ Human research participants
☒	☐ Clinical data

Methods

n/a	Involved in the study
☒	☐ ChIP-seq
☐	☒ Flow cytometry
☒	☐ MRI-based neuroimaging

Antibodies

Antibodies used

Antibodies used in western blot studies:

Primary
Rb anti TRIM37: Bethyl, A301-174A, 1:1000 (Holland, Chapman)
M anti p53: Dako, M7001, 1:1000 (Chapman)
M anti b-actin :Sigma, A1978, 1:1000 (Chapman)
Rb anti 53BP1: Novus Biologicals, NB100-304, 1:2000 (Chapman)
M anti HA-11: BioLegend, 901501, 1:1000 (Chapman)
M anti GST: Sigma, G1160, 1:1000 (Chapman)
Rb anti CEP192: home-made, 1:1000
Rb anti CDK5RAP2: Millipore, 06-1398, 1:2500 (Holland, Chapman)
Rb anti Pericentrin: Abcam, ab4448, 1:2500 (Holland, Chapman)
M anti cyclin A: SantaCruz Biotechnology, sc-53228, 1:1000 (Chapman)
Rb anti phosphorylated Histone H3: Millipore, 06-570, 1:2000 (Chapman)

Secondary
G anti-mouse HRP-conjugated: ThermoFisher Scientific, 31432, 1:1000 (Chapman)
G anti-rabbit HRP-conjugated: ThermoFisher Scientific, 31462, 1:10000 (Chapman)

Antibodies used in Immunofluorescence studies:

M anti Centrin: Millipore, 04-1624, 1:1000 (Holland)

Rb anti CDK5RAP2: Millipore, 06-1398, 1:2500 (Holland)
G anti g-tubulin-Cy5: raised against the following peptide: CDEYHAATRPDYISWGTQEQ, home made, 1:1000
Rb anti Pericentrin: Abcam, ab4448, 1:2500 (Holland)
G anti CEP192-Cy5: raised against CEP192 a.a. 1-211, home made, 1:1000
R anti a-tubulin: ThermoFisher Scientific, MA1-80017, 1:3000 (Holland)
M anti EB1: Santa Cruz, sc-47704, 1:200 (Holland)
S anti CENP-F: a gift from Stephen Taylor at the University of Manchester, 1:2000
M anti phosphorylated Histone H3: Cell Signaling, 9701, 1:2000 (Holland)
Rb anti CEP192: a gift from Karen Oegema at the University of California at San Diego, this study, 1:2000

Antibodies used in flow cytometry studies:

Primary
R anti BrdU-FITC: BioRad, MCA2060FT, 1:100
M anti phosphorylated Histone H3 (Ser10): Cell Signaling, 9706, 1:50

Secondary
G anti-mouse Alexa Fluor 488-conjugated: ThermoFisher Scientific, A-11029, 1:250)

Validation

All of our homemade antibodies were validated by immunoblotting and immunofluorescence to ensure the loss of signal after RNAi depletion or CRISPR/Cas9 knockout of the target protein. When available, we purchased commercial antibodies that have been previously validated in multiple independent studies. Validation procedures used for commercial antibodies are described by the respective manufacturers. In cases where this was not possible, commercial antibodies were validated in house in the same way we validate our homemade antibodies.

All antibodies used in flow cytometry studies were validated by the manufacturers as suitable for use in flow cytometry assays against specific antigens/markers.

Eukaryotic cell lines

Policy information about cell lines

Cell line source(s)

MCF-7 cell lines (WT, TP53BP1-/-, USP28-/-, and TP53-/-) were available in our lab and have been previously described (Cuella-Martin et al., 2016).
HEK293FT, MDA-MB-231, MDA-MB-436, MDA-MB-361 and BT474 cell lines were obtained from the Francis Crick Institute Cell Services.
HCT116 cell line was a gift from Ian Tomlinson.
RPE-1 cell lines, specifically the PLK4AS; TP53-/-; RPE-1 cell line were available in our lab and have been previously described (Lambrus et al., 2016).
DLD-1 and BT549 cell lines were obtained from Stephen Taylor, University of Manchester and Saraswati Sukumar, Johns Hopkins School of Medicine, respectively.

Authentication

MCF-7 cell lines (WT, TP53BP1-/-, USP28-/-, and TP53-/-) have been previously validated (Cuella-Martin et al., 2016), and shRNA expressing lines have been additionally validated by STR profiling.
MDA-MB-231, MDA-MB-436, MDA-MB-361 and BT474 cell lines were validated by STR profiling by the Francis Crick Institute Cell Services.
RPE-1 (WT, TP53BP1-/-, USP28-/-, and TP53-/-) cell lines were validated by western blotting (Supplementary Figure 2) and have been additionally validated by STR profiling.
PLK4AS; TP53-/-; RPE-1 cell line has been previously validated (Lambrus et al., 2016) and have been additionally validated by STR profiling.
HCT116 cell line TP53+/+ and TP53-/- statuses were further validated by western blotting (Extended Data Fig. 1d).
DLD-1 and BT549 cell lines were validated by STR profiling.
HEK293FT cells were used as a packaging cell line for lentiviral production, respectively, and were not further authenticated.

Mycoplasma contamination

Yes - we maintain a very strict regime of mycoplasma testing, and no cell-line tested positive.

Commonly misidentified lines
(See ICLAC register)

We have checked the ICLAC register and the cell lines used in our studies are not on the list of misidentified cell lines.

Human research participants

Policy information about studies involving human research participants

Population characteristics

Adult female patients with breast cancer as part of the BTBC study (see below). This study was limited to working with human tissue samples and data.

Recruitment

Human breast tumour samples were obtained from adult female patients after informed consent as part of a non-interventional clinical trial, the BTBC study, described below.

Ethics oversight

BTBC study: UK National Research Ethics Service - Research Ethics Committee London - (BTBC study REC no.: 13/LO/1248, IRAS

Ethics oversight	ID 131133; Principal Investigator: Prof. Andrew Tutt; Study Title: "Analysis of functional immune cell stroma and malignant cell interactions in breast cancer in order to discover and develop diagnostics and therapies in breast cancer subtypes").

Note that full information on the approval of the study protocol must also be provided in the manuscript.

Flow Cytometry

Plots

Confirm that:

☒ The axis labels state the marker and fluorochrome used (e.g. CD4-FITC).

☒ The axis scales are clearly visible. Include numbers along axes only for bottom left plot of group (a 'group' is an analysis of identical markers).

☒ All plots are contour plots with outliers or pseudocolor plots.

☒ A numerical value for number of cells or percentage (with statistics) is provided.

Methodology

Sample preparation	Cell lines were used for all flow cytometric studies and sourced as indicated above. For sample preparation, cells were trypsinised and washed with 1% BSA in PBS before being fixed in 70% ethanol. Cells were then subjected to staining as described in the methods section.
Instrument	Samples were acquired on an Attune NxT (Life Technologies).
Software	Samples were analysed using FlowJo v10 (Tree Star).
Cell population abundance	Cell sorting was not necessary to evaluate sub-G1 events, cell-cycle phases and ploidy. Thus, it was not performed for these assays.
Gating strategy	Sub-G1/ ploidy analyses: Fixed cells were first gated to exclude debris (FSC-A vs SSC-A), then gated to select for singlets (FSC-H vs FSC-A), and finally assessed for DNA content by Propidium Iodide staining. Cell cycle/mitotic index analyses: Fixed cells were first gated to exclude debris (FSC-A vs SSC-A), then gated to select for singlets (FSC-H vs FSC-A), and finally assessed for DNA content by Propidium Iodide with BrdU or pH3 (negative or negative) stained fractions , when required. Please refer to (Supplementary Figure 3) for figure exemplifying gating the strategies described above.

☒ Tick this box to confirm that a figure exemplifying the gating strategy is provided in the Supplementary Information.